

Euclidean mirrors and first-order changepoints in network time series

Tianyi Chen¹

Zachary Lubberts²

Avanti Athreya³

Youngser Park⁴

Carey E. Priebe⁵

Abstract

We describe a model for a network time series whose evolution is governed by an underlying stochastic process, known as the latent position process, in which network evolution can be represented in Euclidean space by a curve, called the Euclidean mirror. We define the notion of a first-order changepoint for a time series of networks, and construct a family of latent position process networks with underlying first-order changepoints. We prove that a spectral estimate of the associated Euclidean mirror localizes these changepoints, even when the graph distribution evolves continuously, but at a rate that changes. Simulated and real data examples on organoid networks show that this localization captures empirically significant shifts in network evolution.

1 Introduction

Identifying structural changes for a time series of network data is a critical inference task in modern statistics and interdisciplinary data science. For example, in organizational networks, statistical changepoint detection can identify transformations induced by the COVID-19 pandemic in communication patterns of corporations Zuzul et al. [2021]. In brain organoid networks, changepoint detection can distinguish the biologically significant emergence of inhibitory neurons and growth of astrocytes Chen et al. [2023]. As another illustration, spectral network analysis can discern marked fluctuations in global commodity prices in a time series of agricultural trade networks Wang et al. [2023]. In each case, the data is a collection of time-indexed networks, each comprised of nodes and edges, and time series analysis for such network data requires tractably modeling network evolution and managing the inherently non-Euclidean nature of network data.

This non-Euclidean structure, along with the dependency between edges within and across networks, as well as the high dimensionality and noise that accompany Euclidean representations of key network features, all present challenges for the development of principled methodology for network time series. As a consequence, while changepoint analysis for Euclidean data has a rich history Box et al. [2015], Kedem and Fokianos [2005], Padilla et al. [2021], Shumway et al. [2000], Verzelen et al. [2023], time series analysis for networks—indeed, multi-sample network inference more generally—is comparatively new. A natural point of departure is the spectral analysis of a sequence of adjacency matrices or a network tensor: see Agterberg et al. [2022], Athreya et al. [2022], Jing et al. [2021], MacDonald et al. [2022], Padilla et al. [2022], Pantazis et al. [2022], Paul and Chen [2020], Wang et al. [2023] for approaches to the estimation of common parameters, hypothesis testing for differences in networks, and analyses of changepoints and anomalous behavior across networks.

To formalize these ideas, we consider a collection of random networks on the same vertex set, indexed by time. For this network time series, we assume that associated to each vertex i in each network at time

¹Corresponding Author: tchen94@jh.edu; Department of Applied Mathematics and Statistics, Johns Hopkins University

²zlubberts@virginia.edu; Department of Statistics, University of Virginia

³dathrey1@jhu.edu; Department of Applied Mathematics and Statistics; Johns Hopkins University

⁴youngser@jhu.edu; Center for Imaging Science, Johns Hopkins University

⁵cep@jhu.edu; Department of Applied Mathematics and Statistics, Johns Hopkins University

t is a (typically unobserved) low-dimensional vector, called the *latent position*, and that the probability of connections between nodes in the network depends on these latent positions. We assume these latent positions evolve according to some underlying stochastic process. A central question is whether, if the underlying stochastic process—called a *latent position process* (LPP)—changes in some significant way, we can detect this by appropriate analysis of the observed network data itself.

The observed network data consists of a time-indexed collection of adjacency matrices, each entry of which is a Bernoulli random variable with success probability determined by the latent positions of the respective nodes. The observed network adjacency A_t at time t is a noisy version of the matrix of connection probabilities P_t at time t . The matrix of connection probabilities P_t is itself a compression of the information in the underlying realizations of the latent position processes. We do not observe the P_t matrices, much less the realizations of the underlying latent position process. However, because the edge distribution of a latent position network is governed by the latent position process, changepoints for the distribution of the network can be associated to changepoints in the latent position process. Specifically, we consider changes in the distribution of the process itself, which we call *zeroth order* changepoints, as well as changepoints in the distribution of the increments of the process, which we term *higher-order changepoints*. We argue that for real-world networks, evolution in the connection probabilities is the norm, rather than the exception, so the appropriate notion of a changepoint should not be merely a change in the network’s distribution, but rather a change in its pattern of evolution. The relevant inference task, then, is to detect if and when such a change in evolution occurs. This phenomena is subtler than previous methodologies have sought to elucidate.

To localize higher-order changepoints, we follow the methodology in Athreya et al. [2022], where the authors develop a model for time series of networks generated by an underlying LPP and associate to this LPP a finite-dimensional Euclidean curve, called a *mirror*, which provides a Euclidean representation for the network evolution over time. In Athreya et al. [2022], spectral decompositions and classical multidimensional scaling (CMDS) on the observed time series of networks provide consistent estimates of this mirror. When the mirror exhibits manifold structure, nonlinear dimension reduction techniques, such as isometric mapping (ISOMAP) Tenenbaum et al. [2000], yield approximations to this manifold, which we dub the *iso-mirror*. The mirror and iso-mirror represent important features of the LPP and the dynamics of the time series of networks, and shifts in the mirror or iso-mirror can reflect corresponding changes in the latent position process.

Fig 1 presents two real data examples from Athreya et al. [2022] and Chen et al. [2023], with plots of iso-mirrors over time. We observe that in both cases, the iso-mirrors exhibit approximate piecewise linearity. The left panel is the iso-mirror for a time series of communication networks at Microsoft during the initial months of pandemic-induced remote work. A notable linear trend is evident before a significant shift around June 2020 Zuzul et al. [2021]. Similarly, the right panel shows the iso-mirror of inferred effective connectivity for brain organoid connectomes. It too displays a piecewise linear trend with a change in the slope at day 188 Chen et al. [2023], which coincides with the development of inhibitory neurons and the growth of astrocytes.

Motivated in part by this piecewise linearity, we construct a latent position process network with an asymptotically piecewise linear mirror and a first-order changepoint. The LPP is based on a random walk and the first-order changepoint is introduced by shifting the jump probability at t^* from p to $q \neq p$. We prove that the associated mirror converges uniformly, as the number of networks in our times series increases, to a piecewise linear function with a slope change—namely, a higher-order changepoint—at t^* . Therefore, the task of identifying changepoints within network time series translates to analyzing slope changes in the mirror, allowing us to frame changepoint detection in networks as a changepoint analysis problem in Euclidean space. The asymptotic piecewise linearity property of the mirror leads to a localization estimator for t^* , and we prove that this estimator is consistent. We demonstrate this localization procedure on simulated and real data, and show that networks can differ markedly before and after these higher-order changepoints. Higher-order changepoint localization thus enables the discovery of finer changes in network evolution.

1.1 Comparison to previous work

Recent literature on changepoint analysis within time series of graphs (TSG) has significantly expanded. Latent position network models, such as the well-studied random dot product model (RDPG) Agterberg

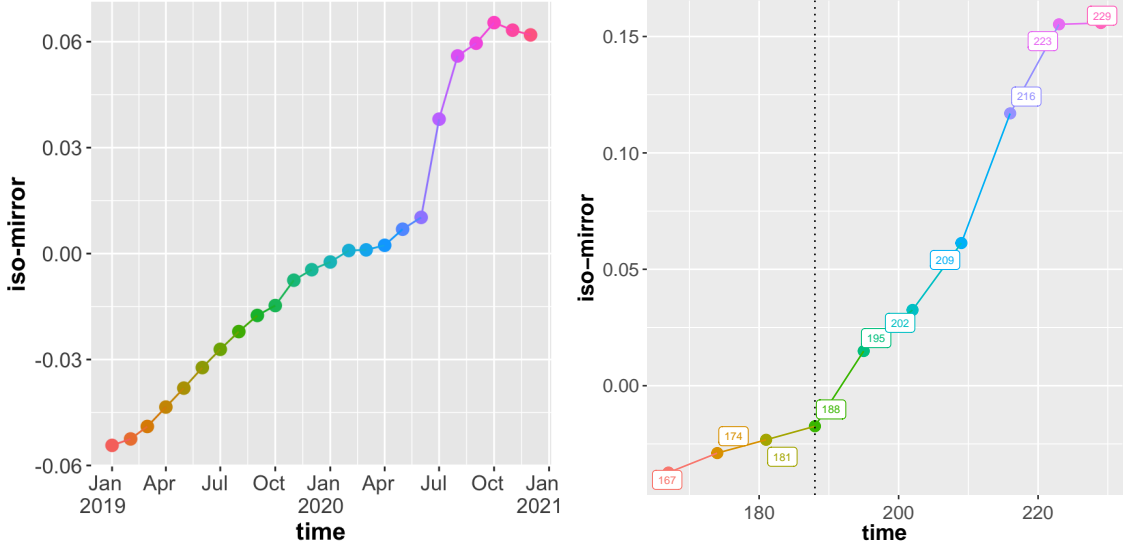


Figure 1: Piecewise linearity appears in real data examples. The left panel shows the iso-mirror estimation for Microsoft’s time series of communication networks. The network is generated each month from 2019 Jan to 2021 Jan. The work-from-home protocols were in effect starting in April 2020. We observe a clear linear trend before April 2020. The right panel is the iso-mirror estimation on time series of brain organoid effective connectivity networks. The networks were sampled roughly once per week and the iso-mirror shows piecewise linearity with a change of slope at day 188.

et al. [2022], Athreya et al. [2022], Jones and Rubin-Delanchy [2020], Kei et al. [2024], Padilla et al. [2022], Wang et al. [2023], are a common point of departure for both individual and joint network analysis. These include the stochastic block model Bhattacharjee et al. [2020], Fan et al. [2022], Padilla et al. [2022], a subset of the RDPG, and more intricate latent space models, such as multiplex and multilayer models Jones and Rubin-Delanchy [2020], MacDonald et al. [2022], Wang et al. [2023].

Of course, in network time series, one must specify more than a generative model for each network at each time point; it is also necessary to describe the dependency between networks at different time points, incorporating potential inter-network dependencies. To address dependency among networks, Jones and Rubin-Delanchy [2020], MacDonald et al. [2022], Wang et al. [2023] propose a shared structural framework for the latent positions of nodes across different layers and times. In MacDonald et al. [2022], it is posited that the latent position matrix for each layer or time is split into initial columns representing common latent positions and subsequent columns for individual latent positions that differ across layers or times. In Wang et al. [2023], the authors consider a multilayer random dot product model where all layers or times share identical latent positions, but the connectivity matrices determining connection probabilities from these latent positions are allowed to vary. Padilla et al. [2022] details how dependencies between networks are modeled by setting the latent positions $X_i(t)$ for a node i at time t as:

$$X_i(t) \begin{cases} = X_i(t-1), & \text{with probability } p, \\ \sim F, & \text{with probability } 1-p, \end{cases}$$

where F is the distribution for the latent position at $t-1$. In Kei et al. [2024], a multi-layer perceptron (MLP) is employed to produce a latent position matrix at each time t from a normal distribution $\mathcal{N}(\mu_t, I_d)$, with MLP parameters shared across times. Additionally, several studies assume independence of networks across layers or times Bhattacharjee et al. [2020], Wang et al. [2021].

To appropriately model changepoints in network time series, we must delineate how network dynamics evolve over time and investigate different types of changepoints; this motivates our definition of changepoints

of different *orders*. At a baseline, a common framework for changepoints in network-time series (see Kei et al. [2024], Padilla et al. [2022], Wang et al. [2021, 2023]) is the model that corresponds, as we define it more formally in Section 2, to a *zeroth-order* changepoint:

Model 1 (Zeroth-order Changepoint). The time series of graphs $\{\mathbf{G}_t\}_{t=1}^m$ having distributions $\{\mathcal{L}_t\}_{t=1}^m$ has a *zeroth-order changepoint* at t^* , $1 < t^* < m$, when

$$\mathcal{L}_{t-1} \neq \mathcal{L}_t \text{ if and only if } t = t^*.$$

In Wang et al. [2021], the underlying probability matrices change only at the changepoints; the authors address detection and localization of an unknown number of changepoints and introduce two methods, both relying on cumulative sum (CUSUM) statistics that necessitate dividing the time series data into two separate series. The authors show that under certain conditions, these methods achieve minimax optimality. Similarly, Padilla et al. [2022] consider a model where the latent position distribution again changes solely at the changepoints. Their algorithm uses spectral methods and CUSUM statistics for localization. In Wang et al. [2023], changepoints in multilayer random dot product models are defined as instances where the connectivity matrices change, also reflecting a zeroth-order changepoint model. The authors develop techniques for online changepoint detection using scan statistics derived from tensor decompositions of the adjacency matrices in the network time series. Meanwhile, Kei et al. [2024] defines a changepoint as a shift in the expected value μ_t of the distribution generating the latent position matrix. The authors determine $\hat{\mu}_t$ using maximum approximate likelihood estimation, incorporating group-fused Lasso regularization, and show that careful analysis of the sequential differences $\hat{\mu}_t - \hat{\mu}_{t-1}$ can effectively detect and localize changepoints.

Here, we consider a time series of networks in which each network is a random dot product graph on the same vertex set with latent positions belonging to the same low-dimensional Euclidean space. We assume the latent positions are samples from a latent position process, with the distributions of these latent positions being dependent across time. A distinctive aspect of our model is that we permit the underlying distribution for networks to drift at each time, with the *rate* of drift altering at the changepoint; this is what we formally define as a first-order changepoint in Section 2. This model renders the algorithms from aforementioned work less effective in localizing our changepoint. Nevertheless, our spectrally-derived estimates of the associated Euclidean mirror for this network time series capture essential signal in the latent position process and lead to intuitive and consistent changepoint localization.

1.2 Organization of paper

We organize the paper as follows. In Section 2, we first introduce our model for network time series; second, we construct a latent position process with a first-order changepoint based on a random walk with a shift in jump probability at a certain time point t^* ; and third, we prove that its associated mirror exhibits an asymptotic piecewise linear structure, with its slope change coinciding with t^* . In Section 3 we use spectral techniques and classical multidimensional scaling, both of which require a choice of embedding dimension, to estimate the mirror based on network observations, and we exploit the asymptotic piecewise linearity of the underlying mirror to construct an l_∞ localization estimator for the changepoint t^* . We prove that when the asymptotic piecewise linearity holds, this changepoint localization is consistent. In numerical experiments, we demonstrate that the estimated iso-mirror can pinpoint the changepoint, even with a limited sample size n . What is more, we investigate the performance of the embedding dimension on the estimated mirror and the estimated changepoint, and see evidence of a bias-variance tradeoff. We also examine a real data time-series of organoid networks, observing a piecewise linear structure for mirror estimates in this data as well, and localizing a changepoint that corresponds to biologically significant shifts in organoid development. In Section 4, we discuss ongoing research and further work. All proofs are in the Appendix.

2 Main model and prior results

2.1 Notation

Consider a vector $v \in \mathbb{R}^d$, which is represented as a column vector. We express v as $v = (v_1, v_2, \dots, v_d)^\top = (v_i)_{i=1}^d$, where v_i denotes the i th entry of v . The vector Euclidean norm is denoted by $\|\cdot\|$. For a matrix $A \in \mathbb{R}^{p_1 \times p_2}$, the element at the i, j th position is represented as $(A)_{i,j}$, and A can be denoted by $[a_{ij}]_{i=1, j=1}^{p_1, p_2}$ with a_{ij} as the entry at the i th row and j th column. The spectral norm of A is denoted by $\|A\|_2$, the Frobenius norm by $\|A\|_F$, the maximum Euclidean row norm by $\|A\|_{2 \rightarrow \infty}$, and the maximum absolute row sum by $\|A\|_\infty$. For a square matrix $A \in \mathbb{R}^{n \times n}$, $\lambda_1(A)$ denotes the largest eigenvalue, $\lambda_2(A)$ the second largest eigenvalue, and so on.

In our asymptotic analysis, we will consider the asymptotic order of various quantities so we introduce the order notation here.

Definition 1 (Order Notation). if $\omega(m)$, $\alpha(m)$ are two quantities depending on m . we will say that ω is of order $\alpha(m)$ and use the notation $\omega(m) \sim \Theta(\alpha(m))$ to mean that there exist positive constants such that for m sufficiently large, $c\alpha(m) \leq \omega(m) \leq C\alpha(m)$. We write $\omega(m) \sim O(\alpha(m))$ if there exists a constant C such that for sufficient large m $\omega(m) \leq C\alpha(m)$.

Additionally we will consider the probabilities of certain events decay at specific rate, so we introduce the notion of convergence with high probability.

Definition 2 (convergence with high probability). Given a sequence of events $\{F_n\} \in \mathcal{F}$, where $n = 1, 2, \dots$, We say that F_n occurs with high probability, and write F_n w.h.p. , if for any $c_0 > 1$, there exists finite positive constant C_0 depending on c_0 such that $\Pr [F_n^c] \leq C_0 n^{-c_0}$ for all n .

2.2 Model formulation and key definitions

Building on the framework for network time series detailed in Athreya et al. [2022], we first define the Random Dot Product Graph (RDPG). For each node i at time t , we assign a corresponding vector in \mathbb{R}^d as latent position. With the latent positions given, the connections between any two nodes are independent, with the connection probability equal to the inner product of their respective latent position vectors. Despite its conceptual straightforwardness, the RDPG model is general enough; as evidenced by Tang et al. [2013], Wolfe and Olhede [2013], with an appropriately high dimensionality d of latent positions, it can effectively approximate any independent edge models.

Definition 3 (Random dot product graph). We say that the undirected random graph G with adjacency matrix $\mathbf{A} \in \mathbb{R}^{n \times n}$ is a *random dot product graph (RDPG)* with latent position matrix $\mathbf{X} \in \mathbb{R}^{n \times d}$, whose rows are the transpositions of the column vectors $X^1, \dots, X^n \in \mathcal{X} \subseteq \mathbb{R}^d$, if

$$\mathbb{P}[\mathbf{A}|\mathbf{X}] = \prod_{i < j} \langle X^i, X^j \rangle^{A_{i,j}} (1 - \langle X^i, X^j \rangle)^{1-A_{i,j}},$$

where $\langle x, y \rangle = x^\top y$ is the inner product between two column vectors. We call $\mathbf{P} = \mathbf{X}\mathbf{X}^\top$ the connection probability matrix. In this case, each A_{ij} is marginally distributed (conditionally on X^i, X^j) as Bernoulli($\langle X^i, X^j \rangle$) and independent of each other.

If instead $\mathbf{P} = \mathbf{X}I_{p,q}\mathbf{X}^\top$, where $I_{p,q} = I_p \oplus (-I_q)$ for some $p + q = d$, we call A a *generalized random dot product graph (GRDPG)*.

Remark 1 (Orthogonal nonidentifiability in RDPGs). Note that if $\mathbf{X} \in \mathbb{R}^{n \times d}$ is a latent position matrix and $\mathbf{W} \in \mathbb{R}^{d \times d}$ is orthogonal, \mathbf{X} and $\mathbf{X}\mathbf{W}$ give rise to the same distribution over graphs. Thus, the RDPG model has a nonidentifiability up to orthogonal transformation. In the case of a GRDPG, \mathbf{X} and $\mathbf{X}\mathbf{W}$ give rise to the same distribution whenever $\mathbf{W}I_{p,q}\mathbf{W}^\top = I_{p,q}$, meaning that \mathbf{W} is an indefinite orthogonal transformation.

In this model each vertex is associated with a column vector, called its *latent position*. And the probability of forming an edge between two vertices is the inner product of two latent positions. To model randomness in the underlying features of each vertex, we will consider latent positions that are themselves random variables defined on a probability space $(\Omega, \mathcal{F}, \mathbb{P})$. Suppose that the time series of networks come from an RDPG model, where at each time t , the latent positions of each vertex are drawn independently from a common distribution F_t . That is, at each time t , the latent positions for n vertices are independent and identically distributed samples drawn from a random variable $X(t)$ which follows the distribution F_t . In order for the inner product to produce a probability between 0 and 1, we require that the distribution of $X(t)$ follows an *inner-product distribution*:

Definition 4 (Inner product distribution). Let F be a probability distribution on \mathbb{R}^d . we call F a *d-dimensional inner product distribution* if $0 \leq x^\top y \leq 1$ for all $x, y \in \text{supp } F$.

Let F be a probability distribution on \mathbb{R}^d . We call F a *d-dimensional generalized inner product distribution* if $d = p + q$, and $0 \leq x^\top I_{p,q} y \leq 1$ for all $x, y \in \text{supp } F$, where $I_{p,q} = I_p \oplus (-I_q)$.

To describe a family of networks indexed by time, each of which is generated by a matrix of latent positions that are i.i.d samples from a random variable, we consider a *latent position stochastic process*.

Definition 5 (Latent position process). A *latent position process* $\varphi(t)$ is a map $\varphi : [0, T] \rightarrow L^2(\Omega)$ such that for each $t \in [0, T]$, $\varphi(t) = X_t$, a random vector in \mathbb{R}^d which has a (generalized) inner product distribution.

Once we have the latent position process, we can construct a time series of RDPGs whose vertices have independent, identically distributed latent positions given by X_t .

Definition 6 (Time series of graphs). Let φ be a latent position process, and fix a given number of vertices n and collection of times $\mathcal{T} \subseteq [0, T]$. We draw an i.i.d. sample $\omega_j \in \Omega$ for $1 \leq j \leq n$, and obtain the latent position matrices $\mathbf{X}_t \in \mathbb{R}^{n \times d}$ for $t \in \mathcal{T}$ by appending the rows $X_t(\omega_j)$, $1 \leq j \leq n$. The *time series of graphs* (TSG) $\{G_t : t \in \mathcal{T}\}$ are conditionally independent RDPGs with latent position matrices $\mathbf{X}_t, t \in \mathcal{T}$.

With this terminology in place, we can now introduce the notion of changepoints of different orders for a time series of networks. We note that much of the existing literature on TSG changepoint detection has focused on the distributions of the networks and how these relate to each other. On the other hand, for a TSG where edges are assumed to arise conditionally independently (at each time and between times), and with a fixed small rank d (or p, q with $p+q = d$) for the mean matrices at each time, there is implicitly a (generalized) latent position process driving the network evolution. As such, it is natural to define changepoints through properties of the LPP, rather than the distributions of the graphs themselves.

Definition 7. A latent position process $\varphi(t)$ is said to have a *zeroth-order changepoint* if there is some $t^* \in [0, T]$ such that

$$X_t - X_{t'} \stackrel{\mathcal{L}}{=} \begin{cases} \delta_0 & \text{if } t, t' \leq t^* \text{ or } t^* \leq t, t' \\ F \neq \delta_0 & \text{otherwise.} \end{cases}$$

Here δ_0 is point mass at $0 \in \mathbb{R}^d$, and F is some other distribution on \mathbb{R}^d .

Define the k th order difference of φ at mesh $\delta > 0$ recursively as follows:

$$\begin{aligned} \Delta_1^\delta(t) &= X_t - X_{t-\delta}, \\ \Delta_k^\delta(t) &= \Delta_{k-1}^\delta(t) - \Delta_{k-1}^\delta(t-\delta). \end{aligned}$$

A latent position process $\varphi(t)$ is said to have a *kth-order changepoint of mesh δ* if there is some $t^* \in [0, T]$ such that

$$\Delta_k^\delta(t) \stackrel{\mathcal{L}}{=} \begin{cases} F_1 & \text{if } t \leq t^*, \\ F_2 & \text{if } t^* + \delta < t, \\ F_3(t) & \text{if } t^* < t \leq t^* + \delta. \end{cases}$$

where we do not have $F_1 = F_2 = F_3(t)$ for all $t \in (t^*, t^* + \delta]$.

Note that a first-order (do we mean zeroth-order) changepoint exactly corresponds to the setting that $\{\varphi(t) : t \in [0, t^*]\}, \{\varphi(t) : t \in (t^* + \delta, T]\}$ are stationary stochastic processes (at least with respect to increments of length δ), but the stationarity breaks down at the point t^* .

We emphasize that each vertex in the TSG corresponds to a single $\omega \in \Omega$, which induces dependence between the latent positions for that vertex across times, but the latent position trajectories of any two distinct vertices are independent of one another across all times.

Since these trajectories form an i.i.d. sample from the latent position process, it is natural to measure their evolution over time using the metric on the corresponding random variables, as described in Athreya et al. [2022]. We reproduce the maximum directional variation metric, d_{MV} , a metric on the space of square-integrable random variables, as follows.

Definition 8. The *maximum directional variation metric* $d_{MV} : L^2(\mathbb{R}^d)^2 \rightarrow [0, +\infty)$ is given by

$$d_{MV}(X_t, X_{t'}) := \min_{W \in \mathcal{O}^{d \times d}} \left\| \mathbb{E}[(X_t - WX_{t'})(X_t - WX_{t'})^\top] \right\|_2^{1/2}, \quad (1)$$

where $\mathcal{O}^{d \times d}$ is the set of all $d \times d$ orthogonal matrices and $\|\cdot\|_2$ is the spectral norm.

In the definition of this distance, the expectation is over $\omega \in \Omega$, which means that it depends on the joint distribution of X_t and $X_{t'}$. In particular, d_{MV} depends on more than just the marginal distributions of the random vectors X_t and $X_{t'}$ individually, but takes into account their dependence inherited from the latent position process φ .

Now we study the geometric properties of the image $\varphi([0, T])$ when equipped with the metric d_{MV} . Often, the map φ admits a Euclidean analogue, called a *mirror*, which is a finite-dimensional curve that retains important signal from the generating LPP for the network time series.

Definition 9 (Exactly Euclidean realizable with mirror ψ). Let φ be a latent position process. We say that φ is *exactly Euclidean c -realizable* with mirror ψ if there exists a Lipschitz continuous curve $\psi : [0, T] \rightarrow \mathbb{R}^c$ such that:

$$d_{MV}(\varphi(t), \varphi(t')) := d_{MV}(X_t, X_{t'}) = \|\psi(t) - \psi(t')\| \text{ for all } t, t' \in [0, T].$$

Remark 2. Exactly Euclidean realizability indicates the pairwise d_{MV} distances between the latent position process at t and t' coincide exactly with Euclidean distances along the curve ψ at t and t' . Hence the term *mirror*, a Euclidean-space curve that replicates the time-varying d_{MV} distance. Sometimes we also use mirror to refer to the image of the curve, and when there are finite times, we refer mirror as the points representing the graphs in Euclidean space.

We can similarly define the approximately Euclidean realizable.

Definition 10 (Approximately Euclidean realizable with mirror ψ). Let φ be a latent position process. For a fixed $\alpha \in (0, 1)$, we say that φ is *approximately α -Hölder Euclidean c -realizable* if ψ is α -Hölder continuous, and there is some $C > 0$ such that

$$\left| d_{MV}(\varphi(t), \varphi(t')) - \|\psi(t) - \psi(t')\| \right| \leq C|t - t'|^\alpha \text{ for all } t, t' \in [0, T].$$

If the LPP is exactly Euclidean realizable, and we sample m time points $\mathcal{T} = \{t_1, t_2, \dots, t_m\} \subseteq [0, T]$, then the corresponding distance matrix

$$(\mathcal{D}_\varphi)_{i,j} := d_{MV}(X_{t_i}, X_{t_j})$$

is *exactly c -Euclidean realizable*, that is, there exists m points $\psi(t_1), \psi(t_2), \dots, \psi(t_m) \in \mathbb{R}^c$ such that

$$(\mathcal{D}_\varphi)_{i,j} = \|\psi(t_i) - \psi(t_j)\| \text{ for all } i, j \in \{1, 2, \dots, m\}.$$

In this case, given \mathcal{D}_φ , classical multidimensional scaling (CMDS) will recover the mirror $\psi(t_1), \psi(t_2), \dots, \psi(t_m)$ exactly up to orthogonal transformation at times t_1, \dots, t_m . CMDS embedding is defined as:

Definition 11 (CMDS embedding to dimension c). Given a distance matrix $\mathcal{D} \in \mathbb{R}^{m \times m}$ and define $P := I - \frac{J_m}{m}$ where I_m is the $m \times m$ identity matrix and J_m is the $m \times m$ all ones matrix. Consider $B := -\frac{1}{2}P\mathcal{D}^{(2)}P$ where $\mathcal{D}^{(2)}$ is the entrywise square of the distance matrix \mathcal{D} . Denote the c largest eigenvalues and corresponding orthogonal eigenvectors of B as $\lambda_1, \dots, \lambda_c$ and u_1, \dots, u_c . Set $\max(\lambda_i, 0) = \sigma_i^2$ and S a diagonal matrix with $S_{ii} := \sigma_i^2$ for $i \in \{1, \dots, c\}$; let $U \in \mathbb{R}^{m \times c} := [u_1 | \dots | u_c]$. Then the output of classical multidimensional scaling (CMDS) \mathcal{D} into dimension c , where $1 \leq c \leq m - 1$, yields m points $\psi(t_1), \dots, \psi(t_m) \in \mathbb{R}^c$, called the c -dimensional CMDS embedding. Put $\psi(t) = (\psi_1(t), \psi_2(t), \dots, \psi_c(t))^\top$ and define Ψ by

$$\Psi := [\psi_j(t_i)]_{i=1, j=1}^{m,c} = \begin{bmatrix} \psi_1(t_1) & \cdots & \psi_c(t_1) \\ \vdots & & \vdots \\ \psi_1(t_m) & \cdots & \psi_c(t_m) \end{bmatrix} = \begin{bmatrix} \psi^\top(t_1) \\ \vdots \\ \psi^\top(t_m) \end{bmatrix} = US^{\frac{1}{2}} = [\sigma_1 u_1 | \dots | \sigma_c u_c].$$

Remark 3. If there are no positive eigenvalues for B , then $S = 0$ and thus $\Psi = 0$. This implies that the distance matrix has no meaningful Euclidean representation. As highlighted in Theorem 1, B must be positive semidefinite for \mathcal{D} to be exactly Euclidean realizable.

We recall, from Trosset and Buyukbas [2020], necessary and sufficient conditions for the distance matrix to be exactly Euclidean realizable:

Theorem 1. *The distance matrix \mathcal{D} is exactly c Euclidean realizable, and is not $c - 1$ Euclidean realizable, if and only if $B = -\frac{1}{2}P\mathcal{D}^{(2)}P$ is positive semidefinite with exactly c positive eigenvalues.*

Definition 12 (Zero-skeleton mirror). Suppose \mathcal{D}_φ is the d_{MV} distance matrix associated with an LPP φ . The output of CMDS applied to \mathcal{D}_φ produces m points in \mathbb{R}^c , denoted $\{\psi(t_1), \dots, \psi(t_m)\}$, called the zero-skeleton c -dimensional (d_{MV}) mirror.

Remark 4. Throughout the paper, $\psi(\cdot) : [0, T] \rightarrow \mathbb{R}^c$, where c is the chosen CMDS embedding dimension, denotes the c -dimensional Euclidean mirror. The image of the function ψ is a c dimensional curve, and $\psi(t) \in \mathbb{R}^c$ provides representation of the graph at time t in c dimensional Euclidean space. When $c > 1$, we use $\psi_k : \mathbb{R} \rightarrow \mathbb{R}$ to denote the k th component of ψ and $[\psi_k(t_i)]_{i=1}^m = \sigma_k u_k$. When we consider m time points, we stack $\{\psi^\top(t_1), \psi^\top(t_2), \dots, \psi^\top(t_m)\}$ row-wise, as a matrix; we denote this as $\Psi \in \mathbb{R}^{m \times c}$.

As we have seen in the analysis of TSGs from multiple application domains, the mirror is often approximately 1-d Euclidean realizable and exhibits piecewise linear structure. In the following section, we introduce a class of LPP models which give rise to an analytically computable, asymptotically piecewise linear mirror with a first-order changepoint, and we use spectral decompositions of the observed networks to localize this changepoint. This holds significant potential for the inference tasks within application domains where an approximate piecewise linear structure in the iso-mirror is observed.

2.3 Random walk latent position process

In this section, we introduce a simple class of LPPs with a closed-form d_{MV} distance. This enables us to analytically compute the mirror obtained through CMDS. The approximate linearity observed in this simple setting will become piecewise-linearity in the later changepoint model.

Model 2 (Random walk latent position process). Let m be an integer, $m \geq 2$. Let t be an integer with $0 \leq t \leq m$. Let $c \geq 0, \delta_m > 0$ be two constants satisfying $c + \delta_m \leq 1$. For a fixed ‘‘jump probability’’ $p \in (0, 1)$, define a LPP φ_m as follows:

$$\begin{aligned} X_0 &= c \quad \text{with probability 1,} \\ \text{For } t \geq 1, \quad X_t &= \begin{cases} X_{t-1} + \delta_m & \text{with probability } p, \\ X_{t-1} & \text{with probability } 1 - p. \end{cases} \end{aligned}$$

We can, of course, express this latent position process as a familiar random walk: let $Z_i, i \geq 1$, be i.i.d random variables defined by $Z_i = \delta_m$ with probability p and $Z_i = 0$ with probability $1 - p$; let $Z_0 = c$ with probability one. Then for $t \in \{0, 1, 2, \dots, m\}$, $X_t = \sum_{k=0}^t Z_k$. Observe that for $t \geq 1$, $X_t - c = V_t \delta_m$, where V_t is a Binomial random variable with t trials and success probability p .

Since $c + \delta_m m \leq 1$, as m increases, δ_m must decrease. For the rest of this section, we consider $X_0 = 0$ and $\delta = \frac{1}{m}$ so that our latent position process is supported on the set $\{0, \frac{1}{m}, \dots, 1\}$. When we consider time series of graphs, it is important for us to take $c > 0, c + \delta_m m < 1$ to ensure sufficient signal strength in each network, but we adopt this choice in the present section for notational simplicity.

The random dot product graph (RDPG) at time t whose vertices have latent positions distributed according to X_t is actually an $(m+1)$ -block stochastic block model (SBM) with block assignment vector $\pi_{t,m,p}$ and block connection probability matrix B_m defined by

$$\pi_{t,m,p}(i) = \begin{cases} \binom{t}{i} p^i (1-p)^{t-i} & \text{for } i \in \{0, 1, 2, \dots, t\} \\ 0 & \text{for } i \in \{t+1, t+2, \dots, m\}, \end{cases}$$

$$B_m(i, j) = \frac{ij}{m^2} \quad \text{where } i, j \in \{0, 1, 2, \dots, m\}.$$

Note B_m is a rank one matrix. It turns out that the d_{MV} distance is analytically tractable for the model 2, and we compute it here.

Lemma 1. *For these latent position process in Model 2,*

$$d_{MV}^2(X_t, X_{t'}) = \left(\frac{p(t-t')}{m} \right)^2 + (p-p^2) \frac{|t-t'|}{m^2} \quad \text{for all } t, t' \in \{1, 2, \dots, m\}. \quad (2)$$

Further we have that Model 2 is approximately $\frac{1}{2}$ -Hölder Euclidean 1-realizable with mirror $\psi(t) = \frac{pt}{m}$:

$$\left| d_{MV}(X_t, X_{t'}) - \|\psi(t) - \psi(t')\| \right| \leq \sqrt{p-p^2} \frac{|t-t'|^{\frac{1}{2}}}{m} \quad \text{for all } t, t' \in \{1, 2, \dots, m\}. \quad (3)$$

Consider the $m \times m$ matrix of pairwise squared distances $\mathcal{D}_{\varphi_m}^{(2)}$:

$$\left(\mathcal{D}_{\varphi_m}^{(2)} \right)_{i,j} = d_{MV}^2(X_i, X_j) = p^2 \left(\frac{i}{m} - \frac{j}{m} \right)^2 + \frac{p-p^2}{m} \left| \frac{i}{m} - \frac{j}{m} \right| \quad \text{where } i, j \in \{1, 2, \dots, m\}.$$

An important consequence of Lemma 1 is that the d_{MV} distance in Equation 2 is the sum of two terms, the first of which is quadratic in the difference between i/m and j/m , and the second of which involves the absolute value of the difference between i/m and j/m , scaled by an additional factor of $1/m$. Consider the case in which $i/m \rightarrow x$ and $j/m \rightarrow y$ as $m \rightarrow \infty$. Here, the second term in the d_{MV} distance is of order $1/m$, but the first term is of constant order, making it the dominant term in the sum. As mentioned above, the first term, a quadratic in the distance between i/m and j/m , is the square of a 1-dimensional Euclidean distance. Hence for large m , we expect that classical multidimensional scaling applied to this dissimilarity will yield, in the first dimension, an approximately linear curve. To illustrate this, we show in Fig 2 the CMDS results for first 3 dimensions when $c = 0.1$, $\delta = \frac{0.9}{m}$, and $m = 40$, $p = 0.4$. The black dots are the output of CMDS on the true distance matrix \mathcal{D}_{φ_m} .

Clearly the 1st dimension of the mirror is close to the linear function $\psi(t) = p(\frac{t}{m} - \frac{1}{2})$ after centering. The second and third dimensions, by contrast, are sinusoidal, but range over an order-of-magnitude smaller scaling: these serve to approximate the diminishing absolute value of the differences encapsulated in the second term of the d_{MV} distance.

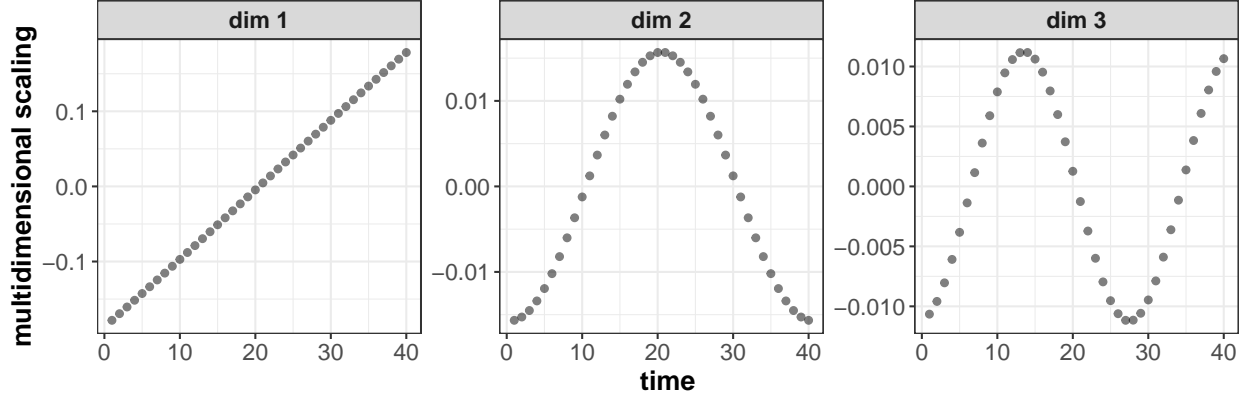


Figure 2: CMDS results on first 3 dimensions for Model 2, while $c = 0.1$, $\delta = \frac{0.9}{m}$, and $m = 40$, $p = 0.4$. The black dots are the numerical CMDS result on the true distance matrix \mathcal{D}_{φ_m} . The left panel, the first dimension of CMDS results clearly shows approximate linearity. The second and third dimensions, by contrast, are sinusoidal, but range over an order-of-magnitude smaller scaling.

2.4 Random walk latent position process with first-order changepoint

Now we have found the 1st dimension of the mirror for the LPP in Model 2. We wish to use the mirror as a tool for subsequent inference by adding a changepoint to the LPP at time t^* and examining whether this is effectively captured by the mirror itself, either in terms of localization of t^* or detection of an underlying distributional change. We will introduce the first-order changepoint by modifying the jump probability, starting at t^* . We set a new, more general LPP φ_m which includes Model 2 as a submodel, but which allows for a change to the jump probability at t^* .

Model 3 (Random walk LPP with first-order changepoint). Let $m \geq 2$ be an integer. Let $c \geq 0, \delta_m > 0$ be constants satisfying $c + \delta_m m \leq 1$. We define the *random walk latent position process with first-order jump probability changepoint at t_m^** by

$$X_0 = c \quad \text{with probability 1,}$$

$$X_t = \begin{cases} X_{t-1} + \delta_m & \text{with probability } p_t \\ X_{t-1} & \text{with probability } 1 - p_t, \end{cases}$$

where $p_t = p$ for $t \leq t_m^*$ and $p_t = q$ for $t > t_m^*$, where $p \neq q$ and $t, t_m^* \in \{1, 2, \dots, m\}$.

Set $c = 0$ and $\delta_m = \frac{1}{m}$; we calculate the d_{MV} distance in this case. Our next lemma exhibits the true mirror for this process.

Lemma 2. *For the latent position process in Model 3,*

$$\left(\mathcal{D}_{\varphi_m}^{(2)}\right)_{i,j} = d_{MV}^2(X_i, X_j) = \begin{cases} p^2 \left(\frac{i}{m} - \frac{j}{m}\right)^2 + \frac{p-p^2}{m} \left|\frac{i}{m} - \frac{j}{m}\right| & i, j < t_m^*, \\ \left(p\left(\frac{t_m^*}{m} - \frac{i}{m}\right) + q\left(\frac{j}{m} - \frac{t_m^*}{m}\right)\right)^2 + \frac{p-p^2}{m} \left|\frac{t_m^*}{m} - \frac{i}{m}\right| + \frac{q-q^2}{m} \left|\frac{j}{m} - \frac{t_m^*}{m}\right| & i < t_m^* < j, \\ q^2 \left(\frac{i}{m} - \frac{j}{m}\right)^2 + \frac{q-q^2}{m} \left|\frac{i}{m} - \frac{j}{m}\right| & t_m^* < i, j. \end{cases}$$

Further we have that Model 3 is approximately $\frac{1}{2}$ -Hölder Euclidean 1-realizable with mirror:

$$\psi(t) = \begin{cases} \frac{pt}{m} & \text{for } t \leq t_m^*, \\ \frac{qt}{m} + \frac{(p-q)t_m^*}{m} & \text{for } t > t_m^*, \end{cases}$$

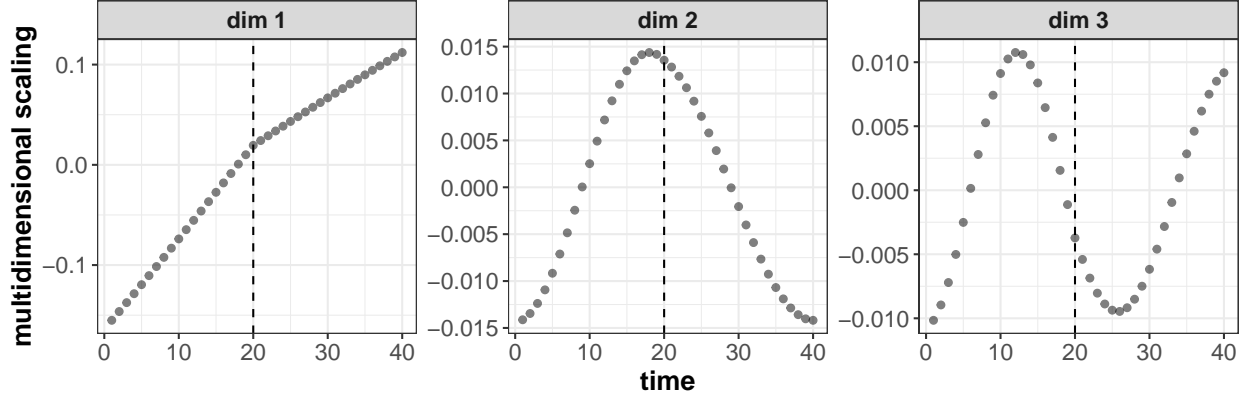


Figure 3: CMDS results on first 3 dimensions for Model 3 while $c = 0.1$, $\delta = \frac{0.9}{m}$ such that the first graph is not too sparse. In this setting $m = 40$, $p = 0.4$, $q = 0.2$, $t_m^* = 20$. The black dots are the numerical CMDS result on $\mathcal{D}_{\varphi_m}^{(2)}$. The approximate piecewise linearity property is observed in dim 1 with slope change at t_m^* . The second and third dimensions also exhibit a change in behavior at t_m^* , where the frequency of the cosine and sine curves changes abruptly, but the range in both sinusoidal terms is an order of magnitude smaller.

and

$$\left| d_{MV}(X_t, X_{t'}) - \|\psi(t) - \psi(t')\| \right| \leq \frac{|t - t'|^{\frac{1}{2}}}{2m} \quad \text{for all } t, t' \in \{1, 2, \dots, m\}. \quad (4)$$

The proof of this lemma is similar to Lemma 1. Observe that similarly to the case without a changepoint, the absolute value terms in this function decrease of order $1/m$ as m grows, leading to an approximately one-dimension squared Euclidean distance, where now the function is piecewise linear instead of linear and the first dimension of the mirror is close to piecewise linear, as shown in Fig 3. Furthermore, the piecewise linear function has a change of slope at t_m^* . This leads us to the next section, where we study the asymptotic behavior of the two models.

2.5 In-fill asymptotics of the mirror

In this section, we consider the behavior of latent position process and associated mirrors as the number of time points m approaches infinity. We note that the time points t_1, \dots, t_m are constrained to lie in a fixed bounded interval, but this interval is sampled increasingly often as m increases. As we show, certain latent position processes can converge to deterministic limits as the number of sampled time points increases. The next lemma guarantees that such deterministic latent position processes satisfy exact Euclidean 1-realizability and have explicitly computable mirrors.

Lemma 3. *If the latent position process $\{\varphi(t)\}$ is deterministic and $t \in (a, b)$, $\varphi(t) \in \mathbb{R}^d$, then it is Exactly Euclidean 1-realizable, with mirror $\psi(t) = \|\varphi(t)\|_2 - \frac{\int_a^b \|\varphi(t)\|_2 dt}{b-a}$.*

We note that for either of these models, as m grows, the discrete time LPP does not append any additional random variables. That is, denoting the LPP with m time-points by $\{X_{t_1}^{(m)}, \dots, X_{t_m}^{(m)}\}$, we have $\{X_{t_1}^{(m)}, \dots, X_{t_m}^{(m)}\} \not\subseteq \{X_{t_1}^{(m+1)}, \dots, X_{t_{m+1}}^{(m+1)}\}$. These are two completely different LPPs and $X_{t_1}^{(m)} \neq X_{t_1}^{(m+1)}$. For example in Model 2, for fixed p , after scaling by m , the LPP is determined by the time points $\{t_1, \dots, t_m\} = \{\frac{1}{m}, \dots, 1\}$; thus as m grows, the times change and in-fill the interval $[0, 1]$.

For Model 2, when $m \rightarrow \infty$, the LPP converges in L_2 to a deterministic LPP. We formalize this with the following lemma.

Lemma 4. Consider $t_{\beta,m} = \lfloor m\beta \rfloor$ with $\beta \in [0, 1]$ fixed as $m \rightarrow \infty$, and denote a continuous deterministic LPP, $\{Z_t\}$, $t \in [0, 1]$ such that $Z_t = tp$ for any t . Then we have $X_{t_{\beta,m}}^{(m)} \xrightarrow{L^2} Z_\beta$.

This coincides with our aforementioned observation for the d_{MV} distance of Model 2 in Lemma 1. Namely $d_{MV}^2 \left(X_{t_{\alpha,m}}^{(m)}, X_{t_{\beta,m}}^{(m)} \right) = p^2(\beta - \alpha)^2 + \frac{p-p^2}{m}|\alpha - \beta| \rightarrow d_{MV}^2(Z_\beta, Z_\alpha)$ as $m \rightarrow \infty$.

The results shown above also hold for Model 3. The latent position process in that case converges in L_2 to the deterministic LPP φ_Z on $[0, 1]$ given by:

$$Z_t = \begin{cases} pt & \text{for } t \leq t^* \\ qt + (p - q)t^* & \text{for } t > t^*, \end{cases}$$

where p, q are the same as before, and $t^* := \frac{t_m^*}{m} \in (0, 1)$ is fixed, $t \in [0, 1]$. By Lemma 3, the mirror ψ_Z associated to Z_t is piecewise linear:

$$\psi_Z(t) = \begin{cases} pt + c_0 & \text{for } t \leq t^* \\ qt + (p - q)t^* + c_0 & \text{for } t > t^*. \end{cases} \quad (5)$$

$$\text{where } c_0 = t^*(p - q) \left(\frac{t^*}{2} - 1 \right) - \frac{q}{2} \text{ such that } \int_0^1 \psi_Z(t) dt = 0.$$

We now define the notion of *asymptotically exactly Euclidean 1-realizable* LPPs:

Definition 13 (In-fill (summably) asymptotically Euclidean 1-realizable). Consider a latent position process X_t , sampled at $0 \leq t_1 < \dots < t_m \leq 1$ and denoted by $\mathcal{X} = \{X_{t_1}^{(m)}, \dots, X_{t_m}^{(m)}\}$, that is exactly Euclidean $(m - 1)$ -realizable with 0-skeleton mirror $\{\psi^{(m)}(t_1), \dots, \psi^{(m)}(t_m)\}$. Define $\tilde{\psi}_1^{(m)}$ to be the piecewise linear interpolation between the points $\left\{ \left(t_i, \psi_1^{(m)}(t_i) \right), 1 \leq i \leq m \right\} \subset \mathbb{R} \times \mathbb{R}$. We say the latent position process X_t is *asymptotically Euclidean 1-realizable with asymptotic mirror* ψ_0 if there exists a function $\psi_0 : [0, 1] \rightarrow \mathbb{R}^1$ such that

$$\sup_{t \in [0, 1]} |\tilde{\psi}_1^{(m)}(t) - \psi_0(t)| \rightarrow 0 \text{ as } m \rightarrow \infty,$$

and

$$\left| d_{MV} \left(X_{t_i}^{(m)}, X_{t_j}^{(m)} \right) - |\psi_0(t_i) - \psi_0(t_j)| \right| \rightarrow 0 \text{ as } m \rightarrow \infty \quad \text{for all } i, j \in \{1, 2, \dots, m\}.$$

Suppose, in addition, that the following conditions hold:

$$\lambda_1 \left(-\frac{1}{2} P \mathcal{D}_m^{(2)} P \right) \sim \Theta(m),$$

$$\frac{\sum_{i=2}^m \lambda_i^2 \left(-\frac{1}{2} P \mathcal{D}_m^{(2)} P \right)}{\lambda_1^2 \left(-\frac{1}{2} P \mathcal{D}_m^{(2)} P \right)} \rightarrow 0,$$

where $(\mathcal{D}_m)_{i,j} = d_{MV} \left(X_{t_i}^{(m)}, X_{t_j}^{(m)} \right)$. In this case, we call the latent position process *summably asymptotically Euclidean 1-realizable*.

An asymptotically Euclidean 1-realizable LPP is such that the first dimension of the mirror uniformly converges to the one-dimensional curve ψ_0 , which asymptotically matches the distances in \mathcal{D}_m ; we can naturally extend this definition to asymptotically Euclidean d -realizable.

Asymptotic realizability is concerned with the behavior, as m increases, of the latent position process defined for the points t_1, \dots, t_m in the unit interval, which is a fixed, bounded interval. Since the number of points t_i in this interval increases, we consider a time rescaling of Model 3 with changepoints t_m^* satisfying $t_m^* = t^*m$ for some fixed $t^* \in (0, 1)$. This leads us to the notion of an *in-fill random walk latent position process with changepoint*.

Model 4 (In-fill random walk LPP with changepoint). Let $t^* \in (0, 1)$. For any $m \geq 2$, set $c = 0$, $\delta_m = 1/m$, and let $\tilde{X}_t^{(m)}$ follow the random walk LPP of Model 3 with first-order jump probability changepoint at $t_m^* = \lfloor t^* m \rfloor$. Put $t_i = i/m$ for $i \in \{1, \dots, m\}$ and define the *in-fill random walk LPP with changepoint at t^** as

$$X_{t_i}^{(m)} = \tilde{X}_i^{(m)}, 1 \leq i \leq m.$$

That is,

$$X_0^{(m)} = 0 \quad \text{with probability 1,}$$

$$X_{t_i}^{(m)} = \begin{cases} X_{t_{i-1}}^{(m)} + \frac{1}{m} & \text{with probability } p_{t_i} \\ X_{t_{i-1}}^{(m)} & \text{with probability } 1 - p_{t_i}, \end{cases}$$

where $p_{t_i} = p$ for $t_i \leq t^*$ and $p_{t_i} = q$ for $t_i > t^*$.

Observe that the distance matrix for Model 4 is

$$\left(\mathcal{D}_{\varphi_m}^{(2)}\right)_{i,j} = \begin{cases} \frac{p^2}{m^2}(i-j)^2 + \frac{p-p^2}{m^2}|i-j| & i, j < t_m^*, \\ \left(\frac{p}{m}(t_m^* - i) + \frac{q}{m}(j - t_m^*)\right)^2 + \frac{p-p^2}{m^2}(t_m^* - i) + \frac{q-q^2}{m^2}(j - t_m^*) & i < t_m^* < j, \\ \frac{q^2}{m^2}(j-i)^2 + \frac{q-q^2}{m^2}|i-j| & t_m^* < i, j. \end{cases}$$

With ψ_Z as given in Eq. (5), we define the squared dissimilarity matrix $\mathcal{D}_Z^{(2)}$ as follows:

$$\left(\mathcal{D}_Z^{(2)}\right)_{i,j} = \left(\psi_Z\left(\frac{i}{m}\right) - \psi_Z\left(\frac{j}{m}\right)\right)^2 = \begin{cases} \frac{p^2}{m^2}(i-j)^2 & i, j < t_m^*, \\ \left(\frac{p}{m}(t_m^* - i) + \frac{q}{m}(j - t_m^*)\right)^2 & i < t_m^* < j, \\ \frac{q^2}{m^2}(i-j)^2 & t_m^* < i, j. \end{cases}$$

As mentioned above, we observe that

$$\left(\mathcal{D}_Z^{(2)} - \mathcal{D}_{\varphi_m}^{(2)}\right)_{i,j} \sim O\left(\frac{1}{m}\right) \quad \text{for all } i, j \in \{1, 2, \dots, m\}.$$

We focus on two main results on changepoint localization. The first, Theorem 2, guarantees that as $m \rightarrow \infty$, the changepoint LPP in Model 4 is summably asymptotically Euclidean 1-realizable with a piecewise linear asymptotic mirror. The second pair of results, Theorem 6 and 8 in Section 3.2, show that spectral methods can consistently locate this change point. Theorem 2, below, asserts that the asymptotic mirror associated for the LPP in Model 4 has piecewise linear structure with a change in slope at the LPP changepoint, reinforcing the core idea that the Euclidean mirror (or its asymptotic variant) captures core features of the underlying network evolution.

Theorem 2 (Model 4 is summably asymptotically Euclidean 1-realizable with piecewise linear asymptotic mirror). *Consider the in-fill random walk latent position process in Model 4 with changepoint at $t^* \in (0, 1)$. This LPP is summably asymptotically Euclidean 1-realizable with asymptotic mirror given by the piecewise linear function ψ_Z :*

$$\psi_Z(t) = \begin{cases} pt + c_0 & \text{for } t \leq t^* \\ qt + (p-q)t^* + c_0 & \text{for } t > t^*. \end{cases}$$

$$\text{where } c_0 = t_m^* (p - q) \left(\frac{t_m^*}{2} - 1\right) - \frac{q}{2} \text{ such that } \int_0^1 \psi_Z(t) dt = 0.$$

Namely, the following four properties hold:

(1) there exist $w_m \in \{\pm 1\}$ such that $\sup_{t \in [0, 1]} |\tilde{\psi}_1^{(m)}(t) - w_m \psi_Z(t)| \rightarrow 0$ as $m \rightarrow \infty$,

- (2) $\max_{i,j \in \{1,2,\dots,m\}} \left(\mathcal{D}_{\varphi_m}^{(2)} - \mathcal{D}_Z^{(2)} \right)_{i,j} \rightarrow 0$ as $m \rightarrow \infty$,
- (3) $\tilde{\lambda}_1 \sim \Theta(m)$, where $\tilde{\lambda}_1, \tilde{\lambda}_2, \dots, \tilde{\lambda}_m$ are eigenvalues of $-\frac{1}{2}P\mathcal{D}_{\varphi_m}^{(2)}P$,
- (4) $\frac{\sum_{i=2}^m \tilde{\lambda}_i^2}{\tilde{\lambda}_1^2} \rightarrow 0$ as $m \rightarrow \infty$.

This theorem guarantees the piecewise linearity of the asymptotic mirror ψ_Z for the LPP in Model 4 and also shows that the jump probability changepoint t^* of the underlying LPP coincides with the slope changepoint in the asymptotic mirror ψ_Z . Next, we use this observation to consistently localize the changepoint from an observed time series of networks coming from such an LPP.

3 Changepoint analysis

In Model 4, at the changepoint t^* , the jump probability changes in the LPP itself. As we defined in Definition 7, this is a first order changepoint for the LPP. Indeed, for a fixed m and any $i \in \{1, 2, \dots, m\}$:

$$\Delta_{\mathbf{1}}^{\frac{1}{m}}(t_i) \stackrel{\mathcal{L}}{=} \begin{cases} \frac{1}{m} Z_p & \text{if } t_i \leq t^*, \\ \frac{1}{m} Z_q & \text{if } t^* + \frac{1}{m} < t_i, \\ \frac{1}{m} Z_q & \text{if } t^* < t_i \leq t^* + \frac{1}{m}, \end{cases}$$

where Z_p is a Bernoulli random variable with success probability p . In this section, we adapt techniques from Athreya et al. [2022] to show that network realizations from the in-fill LPP model (Model 4) can be used to estimate Euclidean mirrors and localize changepoints associated to the underlying latent position process.

3.1 Estimation of model parameters from network realizations

Our network time series consists of time-indexed graphs on a common vertex set, and for any given time, each vertex has a corresponding time-dependent latent position. The latent positions are typically unknown, but can be consistently estimated through spectral decompositions of the observed adjacency matrices Sussman et al. [2012]. Suppose that G is a random dot product graph with latent position matrix $\mathbf{X} \in \mathbb{R}^{n \times d}$, where the rows of \mathbf{X} are independent, identically distributed draws from a latent position distribution F on \mathbb{R}^d . Let $\mathbf{P} = \mathbf{X}\mathbf{X}^T$ be the connection probability matrix and \mathbf{A} be the adjacency matrix for this graph. The *adjacency spectral embedding* (ASE) is a rank d eigendecomposition of the adjacency matrix.

Definition 14 (Adjacency Spectral Embedding). Given an adjacency matrix \mathbf{A} , we define the *adjacency spectral embedding* (ASE) with dimension d as $\hat{\mathbf{X}} = \hat{\mathbf{U}}|\hat{\mathbf{S}}|^{1/2}$, where $\hat{\mathbf{S}} \in \mathbb{R}^{d \times d}$ is the diagonal matrix with the d largest eigenvalues of \mathbf{A} in magnitude on its diagonal, arranged in decreasing order. $\hat{\mathbf{U}} \in \mathbb{R}^{n \times d}$ is the matrix of d corresponding orthonormal eigenvectors arranged in the same order. $\hat{\mathbf{X}}$ is the estimated latent position matrix.

When the true dimension d of the latent positions—or equivalently, the rank of \mathbf{P} —is unknown, we can infer it using the scree plot Zhu and Ghodsi [2006]. The ASEs of the observed adjacency matrices in our TSG at times t and s , denoted $\hat{\mathbf{X}}_t$ and $\hat{\mathbf{X}}_s$, are estimates of the latent position matrices \mathbf{X}_t and \mathbf{X}_s , from which we obtain an estimate \hat{d}_{MV} , defined below, of the d_{MV} distance between the latent position random variables over time.

Definition 15. The *estimated* d_{MV} distance \hat{d}_{MV} is defined as

$$\hat{d}_{MV}(\hat{\mathbf{X}}_t, \hat{\mathbf{X}}_s) := \min_{W \in \mathcal{O}^{d \times d}} \frac{1}{\sqrt{n}} \|\hat{\mathbf{X}}_t - \hat{\mathbf{X}}_s W\|_2.$$

In Athreya et al. [2022], the authors show that \hat{d}_{MV} is a consistent estimate for the true dissimilarity.

Theorem 3. *Athreya et al. [2022] With overwhelming probability,*

$$\left| \hat{d}_{MV}(\hat{\mathbf{X}}_t, \hat{\mathbf{X}}_s)^2 - d_{MV}(\varphi(t), \varphi(s))^2 \right| \leq \frac{\log(n)}{\sqrt{n}}.$$

Sampling our network time series at m time points, we obtain m adjacency matrices whose spectral embeddings yield the matrix $\hat{\mathcal{D}}$ of pairwise estimated dissimilarities:

$$\left(\hat{\mathcal{D}}_\varphi \right)_{s,t} = \hat{d}_{MV}(\hat{\mathbf{X}}_s, \hat{\mathbf{X}}_t).$$

As in Definition 11, let $P := I_m - \frac{J_m}{m}$ where I_m is the $m \times m$ identity matrix and J_m is the $m \times m$ all ones matrix. Recall from Definition 12 that the c -dimensional zero-skeleton mirror ψ for the latent position process φ is given by the rows of $US^{1/2}$, where S is the diagonal matrix of the c largest positive eigenvalues of $-\frac{1}{2}P\mathcal{D}_\varphi^{(2)}P^\top$ and U the matrix of associated eigenvectors. Since $\hat{\mathcal{D}}_\varphi$ serves as a reasonable estimate for \mathcal{D} , we apply classical multidimensional scaling of this estimated dissimilarity matrix to generate an estimated zero-skeleton mirror.

Definition 16 (Estimated zero-skeleton mirror). Let $\hat{\lambda}_1, \dots, \hat{\lambda}_c$ denote the c largest eigenvalues, in decreasing order, of $\hat{\mathcal{D}}_\varphi$. Put $\hat{S}_{ii} = \max\{\lambda_i, 0\}$. Let \hat{U} be the ordered matrix of eigenvectors associated to the c largest eigenvalues of $\hat{\mathcal{D}}_\varphi$. Let $\hat{\psi}(t_k)$ denote the k th row of $\hat{U}\hat{S}^{1/2}$. The *estimated c -dimensional zero skeleton mirror* is given by $\{\hat{\psi}(t_1), \dots, \hat{\psi}(t_m)\}$.

The following theorem from Athreya et al. [2022] allows us to control the error between the true and estimated zero-skeleton mirror.

Theorem 4 (Control between mirror and estimated mirror). *Suppose \mathcal{D}_φ is approximately c Euclidean realizable. Let $\hat{U}, U \in \mathbb{R}^{m \times c}$ be the top c eigenvectors, and $\hat{S}, S \in \mathbb{R}^{c \times c}$ be the diagonal matrices with diagonal entries equal to the top c eigenvalues of $-\frac{1}{2}P\hat{\mathcal{D}}_\varphi^{(2)}P^\top$ and $-\frac{1}{2}P\mathcal{D}_\varphi^{(2)}P^\top$, respectively. Suppose $S_{i,i} > 0$ for $1 \leq i \leq c$. Then there is a constant C such that with overwhelming probability, there is a real orthogonal matrix $R \in \mathcal{O}^{c \times c}$ such that*

$$\|\hat{U}\hat{S}^{1/2} - US^{1/2}R\|_F \leq \frac{C}{\lambda_c(-\frac{1}{2}P\mathcal{D}_\varphi^{(2)}P^\top)} \left(\frac{m \log(n)}{\sqrt{n}} + \sqrt{\sum_{i=c+1}^m \lambda_i^2 \left(-\frac{1}{2}P\mathcal{D}_\varphi^{(2)}P^\top \right)} \right).$$

In particular, we have

$$\max_{1 \leq i \leq m} \|\hat{\psi}(t_i) - R\psi(t_i)\|^2 \leq \sum_{i=1}^m \|\hat{\psi}(t_i) - R\psi(t_i)\|^2 \leq \frac{C}{\lambda_c^2(-\frac{1}{2}P\mathcal{D}_\varphi^{(2)}P^\top)} \left(\frac{m \log(n)}{\sqrt{n}} + \sqrt{\sum_{i=c+1}^m \lambda_i^2 \left(-\frac{1}{2}P\mathcal{D}_\varphi^{(2)}P^\top \right)} \right)^2.$$

The results above guarantee that for a fixed number of graphs m in the TSG, as the number of vertices tends to infinity, at time t_i , the estimated mirror $\hat{\psi}(t_i)$ will be close to the true mirror $\psi(t_i)$ in the low dimensional Euclidean space. This is depicted in Figure 4, where, with $n = 1500$, the estimated mirror (blue dots) precisely aligns with the true mirror (black dots) in the first dimension. In the second dimension, the alignment of the estimated mirrors is less accurate, and the discrepancy increases further in the third dimension.

We will leverage these results to show the consistency of localizing the changepoint using TSG realizations in the Section 3.2.

3.2 Consistency of the localizing estimator

3.2.1 Consistency for exactly Euclidean 1-realizable latent position processes

In the following sections, we operate under the assumption that there is a single first-order changepoint, as outlined in Model 4, i.e., $p \neq q$. Our primary objective is to localize this changepoint as opposed

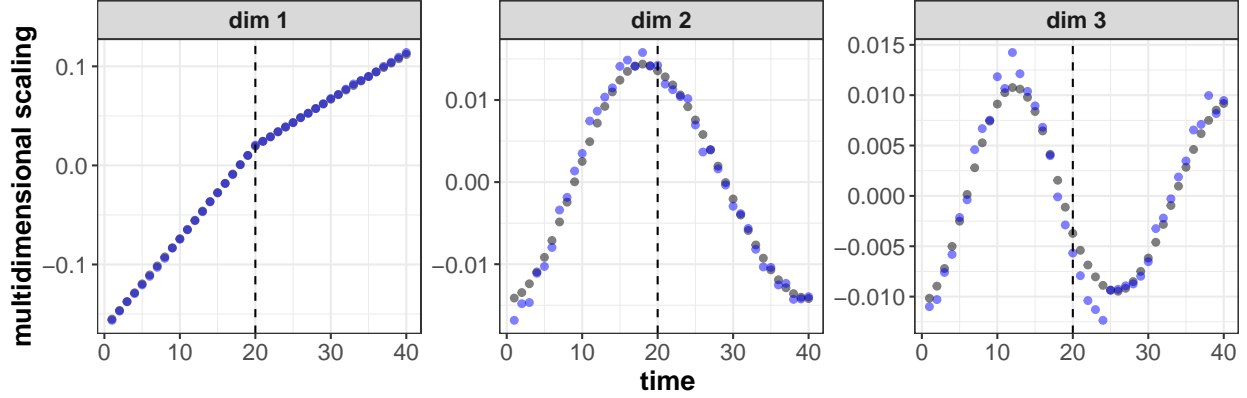


Figure 4: CMDS results on first 3 dimensions for Model 3 with same setting as in Figure 3. The black dots are the numerical CMDS result on $\mathcal{D}_{\varphi_m}^{(2)}$. The blue dots are estimation from one realization of time series of graphs with $n = 1500$. Blue dots precisely aligns with the black dots in the first dimension. In the second dimension, the alignment of the estimated mirrors is less accurate, and the discrepancy increases further in the third dimension.

to detecting whether there is a changepoint. We first consider a simpler case, where the LPP is exactly Euclidean realizable with a piecewise linear mirror. Specifically, consider an exactly Euclidean 1-realizable latent position process with the mirror ψ defined by:

$$\psi(t) = \begin{cases} pt & \text{for } t < t^*, \\ qt + (p - q)t^* & \text{for } t \geq t^* \quad p \neq q. \end{cases}$$

This is equivalent to

$$\psi(t) = pt + (q - p)(t - t^*)I_{\{t > t^*\}} \quad t \in [0, T], t^* \in (0, T) \quad p \neq q.$$

This mirror is a continuous piecewise linear function with the slope change at t^* . Consider the time series of networks on n vertices at points $\mathcal{T} = \{t_1, \dots, t_m\}$ with this latent position process. Let $\{\hat{\psi}(t_i) | 1 \leq i \leq m\}$ denote the spectrally-derived estimated mirror of Athreya et al. [2022]. Our goal is to localize t^* using $\hat{\psi}$. Throughout the section, without loss of generality, we will assume $t_1 = 0$ and $t_m = T$. That is the sampled time points will always include the endpoints.

To localize t^* we propose a simple localization estimator based on l_∞ regression and show its consistency. Without loss of generality, we can consider $p = 0$, $\Delta = q - p > 0$; that is:

$$\psi(t) = \Delta(t - t^*)I_{\{t > t^*\}} \quad t \in [0, T].$$

Let \mathcal{S} be the class of all continuous piecewise linear function with exactly one changepoint on $[0, T]$:

$$\mathcal{S} = \{f | f(t) = \alpha + \beta_L(t - t') + (\beta_R - \beta_L)(t - t')I_{\{t > t'\}} \quad t \in [0, T]; t', \alpha, \beta_L, \beta_R \in \mathbb{R}, \beta_L \neq \beta_R\}.$$

Let $\mathcal{S}(\mathcal{T}) \subseteq \mathcal{S}$ be the subclass of continuous, piecewise linear functions on $[0, T]$ whose unique changepoint belongs to the set $\{t_1, \dots, t_m\}$:

$$\mathcal{S}(\mathcal{T}) = \{f | f(t) = \alpha + \beta_L(t - t') + (\beta_R - \beta_L)(t - t')I_{\{t > t'\}} \quad t \in [0, T]; t' \in \mathcal{T}, \alpha, \beta_L, \beta_R \in \mathbb{R}, \beta_L \neq \beta_R\}.$$

Let $\tilde{\psi}$ as the continuous, piecewise linear interpolation between the points $\{(t_i, \hat{\psi}(t_i)), t_i \in \mathcal{T}\}$. Consider the following minimization problem:

$$\min_{f \in \mathcal{S}(\mathcal{T})} \sup_{t \in [0, T]} |f - \tilde{\psi}(t)|. \quad (6)$$

We claim the following.

Lemma 5. Consider two continuous piecewise linear functions f_1 and f_2 defined on $x \in [a, b]$, and each with a finite collection of changepoint sets denoted, respectively, by $\{t_1, t_2, \dots, t_m\} = \mathcal{T}_1$ and $\{t'_1, t'_2, \dots, t'_n\} = \mathcal{T}_2$. Suppose $\mathcal{T} = \mathcal{T}_1 \cup \mathcal{T}_2$. Then

$$\sup_{x \in [a, b]} |f_1(x) - f_2(x)| = \max\{|f_1(a) - f_2(a)|, \max_{x \in \mathcal{T}} |f_1(x) - f_2(x)|, |f_1(b) - f_2(b)|\},$$

namely, the uniform norm of difference of two piecewise linear functions on an interval are determined only by their changepoints and endpoints of the interval.

Thus by Lemma 5 we show that Eq (6) is equivalent to minimizing the problem below as $t_1 = 0$ and $t_m = T$:

$$\min_{f \in \mathcal{S}(\mathcal{T})} \max_{t \in \mathcal{T}} |f(t) - \hat{\psi}(t)|.$$

Let $h = h_{\hat{\psi}}$ be the minimizer in Eq (6). Note that h is given by,

$$h = \arg \min_{f \in \mathcal{S}(\mathcal{T})} \max_{t \in \mathcal{T}} |f(t) - \hat{\psi}(t)|.$$

Generating h involves selecting an optimal time in \mathcal{T} as well as parameters of the piecewise linear function before and after the changepoint, to satisfy:

$$\hat{t}, \hat{\alpha}, \hat{\beta}_L, \hat{\beta}_R = \arg \min_{\substack{t' \in \mathcal{T} \\ \alpha, \beta_L, \beta_R, \beta_L \neq \beta_R}} \max_{t \in \mathcal{T}} |\alpha + \beta_L(t - t') + (\beta_R - \beta_L)(t - t')I_{\{t > t'\}} - \hat{\psi}(t)|. \quad (7)$$

In practice if such \hat{t} is not unique, we will choose the earliest time that minimizes the objective function, that is:

$$\hat{t} = \min \{t' : (t', \cdot) \in \arg \min_{\substack{t' \in \mathcal{T} \\ \alpha, \beta_L, \beta_R, \beta_L \neq \beta_R}} \max_{t \in \mathcal{T}} |\alpha + \beta_L(t - t') + (\beta_R - \beta_L)(t - t')I_{\{t > t'\}} - \hat{\psi}(t)|\}. \quad (8)$$

This \hat{t} is our changepoint localization estimator, called the l_∞ localization estimator. This estimator considers every time point $t' \in \mathcal{T}$ and sets it as a candidate changepoint, then fits the best piecewise-linear function with knot at t' to the given data, with respect to the l_∞ norm. Then we calculate the infinity loss $\ell(t')$, and choose the least candidate changepoint which minimizes $\ell(t')$. We summarize this procedure in Algorithm 1. Note that \hat{t} is the same whether we use $\{\hat{\psi}(t_i) | 1 \leq i \leq m\}$ or $\{-\hat{\psi}(t_i) | 1 \leq i \leq m\}$.

Algorithm 1 l_∞ localization for piecewise linear data

- 1: Input: m pairs of observations $\{(t_1, y_1), (t_2, y_2), \dots, (t_m, y_m)\}$ with each $t_i \in \mathbb{R}, y_i \in \mathbb{R}$.
- 2: **for** k **from** 2 **to** $m - 1$:
- 3: Define

$$S_k := \min_{\alpha, \beta_L, \beta_R \in \mathbb{R}, \beta_L \neq \beta_R} \max_{1 \leq i \leq m} |\alpha + \beta_L(t_i - t_k) + (\beta_R - \beta_L)(t_i - t_k)I_{\{t_i > t_k\}} - y_i|.$$

- 4: Find the smallest k_0 such that $S_{k_0} = \min\{S_2, S_3, \dots, S_{m-1}\}$ and set $\hat{t} = t_{k_0}$.
 - 5: Output: \hat{t} .
-

We prove in the following lemma that we can upper bound the difference between \hat{t} and the true changepoint t^* .

Lemma 6. With ψ and $\tilde{\psi}$ defined as above, and

$$\max_{1 \leq i \leq m-1} |t_i - t_{i+1}| = \rho,$$

then

$$|\hat{t} - t^*| \leq \left(\frac{4 \min_{w \in \{\pm 1\}} \sup_{t \in [0, T]} |\tilde{\psi}(t) - w\psi(t)|}{\Delta} + 2\rho \right) \frac{T}{\min\{T - t^*, t^*\}}.$$

Utilizing the piecewise linear property of $\tilde{\psi}$ and Theorem 4, we can control $\sup_{t \in [0, T]} |\tilde{\psi}(t) - \psi(t)|$ with the following theorem:

Theorem 5. *Assume a LPP is exactly Euclidean 1-realizable with mirror $\psi(t)$, which is α -Hölder continuous with constant L on $t \in [0, T]$. Consider the estimated mirror $\{\hat{\psi}(t_i) | 1 \leq i \leq m\}$ from the TSG which is generated from this LPP with number of vertices n . Denote $\tilde{\psi}(t)$ the piecewise linear interpolation between the points $\{(t_i, \hat{\psi}(t_i)), 1 \leq i \leq m\}$. Also assume $t_1 = 0$, $t_m = T$, $\max_{1 \leq i \leq m} |t_i - t_{i+1}|^\alpha = \rho$. Then there is a constant C and a $w_m \in \{\pm 1\}$ such that with high probability:*

$$\sup_{t \in [0, T]} |\tilde{\psi}(t) - w_m \psi(t)| \leq \rho L + C \frac{m \log(n)}{\sqrt{n} \lambda_1 \left(-\frac{1}{2} P \mathcal{D}^{(2)} P\right)},$$

where $\mathcal{D}^{(2)}$ is the $m \times m$ entrywise square of the distance matrix of the mirror $\psi(t)$, namely $\mathcal{D}_{ij}^{(2)} = \|\psi(t_i) - \psi(t_j)\|^2$ and $P = I - J/m$, where J is the $m \times m$ matrix with all entries equal to 1.

Combining these results, we see that the l_∞ localization estimator is consistent for the true changepoint t^* .

Theorem 6. *Consider an exactly Euclidean 1-realizable latent position process with mirror $\psi(t) = \Delta(t - t^*)I_{\{t > t^*\}}$ $t \in [0, T]$, $\Delta > 0$ and $\psi_{centered}(t) = \Delta(t - t^*)I_{\{t > t^*\}} + \Delta\left(t^* - \frac{T^2 - (t^*)^2}{2T}\right)$ is the centered version such that $\int_0^T \psi_{centered}(t) dt = 0$. Consider the time series of networks on n vertices at points $\mathcal{T} = \{t_1, \dots, t_m\}$ with this latent position process. Assume $t_1 = 0$, $t_m = T$, and $t^* \in (t_1, t_m)$. Let $\{\hat{\psi}(t) | t \in \mathcal{T}\}$ denote the spectrally-derived estimated mirror of Athreya et al. [2022]. Let $\rho = \max_{1 \leq i < m} |t_i - t_{i+1}|$. Let \hat{t} be the l_∞ localization estimator in Eq.(7), namely:*

$$\hat{t}, \hat{\alpha}, \hat{\beta}_L, \hat{\beta}_R = \arg \min_{t' \in \mathcal{T}} \max_{\alpha, \beta_L, \beta_R, \beta_L \neq \beta_R} |\alpha + \beta_L(t - t') + (\beta_R - \beta_L)(t - t')I_{\{t > t'\}} - \hat{\psi}(t)|.$$

Then there exists a constant C such that with high probability:

$$|\hat{t} - t^*| \leq \left(\frac{Cm \log(n)}{\left(\sum_{i=1}^m \psi_{centered}^2(t_i)\right) \Delta \sqrt{n}} + 6\rho \right) \frac{T}{\min\{T - t^*, t^*\}}.$$

Corollary 1. *When we uniformly sample the time points in $[0, T]$, that is, for any $1 \leq i < m$, $t_{i+1} - t_i = \frac{T}{m-1}$, then for large m and n , there exists a constant C such that with high probability:*

$$|\hat{t} - t^*| \leq \left(\frac{C \log(n)}{\Delta^3 \sqrt{n}} + \frac{6T}{m-1} \right) \frac{T}{\min\{T - t^*, t^*\}}.$$

The upper bound shows the performance of \hat{t} is determined by the the change in slope of the mirror at the changepoint, as measured by Δ , as well as the number of time points m , which determines how the fineness of the mesh, and the size of the graphs n , which determines the noise in the estimation of ψ . Another key point in this bound is the dependence on $\min\{t^*/T, 1 - t^*/T\}$, which measures how close the changepoint is to either of the endpoints of the interval. When this quantity is small, there are fewer time points which can be used to determine the slope of the line segments before and after the changepoint, leading to a harder estimation problem for the mirror, and thus the changepoint itself.

A weakness of the given bound is the first term within the parentheses, which captures the noise in the estimation of $\psi(t)$ at a given time-point. Since the sample size grows with the number of time points, one

might suppose that even with a constant amount of variance in each estimate $\hat{\psi}(t)$ for $\psi(t)$, as m grows, the error between the learned function (h) and the true one (ψ) should go to 0, which would cause this term to disappear. However, analysis of this term requires very delicate analysis of the output of CMDS under multiple sources of error: We have error arising from the finite number of time points m ; error from the finite number of vertices even if we knew the true latent position matrices, in the estimation of d_{MV} ; and error from the finite number of vertices because we have to estimate the latent position matrices from the observed adjacency matrices. As such, the errors between entries of the computed distance matrix and the truth are dependent, and this weakens the benefit of increasing m when there is a fixed, positive amount of variance in each of the estimates $\hat{\psi}(t)$.

3.2.2 Consistency for in-fill summably asymptotically Euclidean 1-realizable model

In this section, we will generalize the above result for exactly Euclidean 1-realizable LPPs to the setting of in-fill summably asymptotically Euclidean 1-realizable LPPs where the asymptotic mirror is piecewise linear with a changepoint at t^* as in definition 13.

First we can adapt Theorem 5 to this situation.

Theorem 7. *Assume an LPP is in-fill asymptotically 1-Euclidean realizable with the 0-skeleton mirror $\{\psi^{(m)}(t_i), 1 \leq i \leq m\}$, and the asymptotic mirror $\psi_0(t)$. Denote $\tilde{\psi}_1^{(m)}(t)$ as the piecewise linear interpolation between the points $\{(t_i, \psi_1^{(m)}(t_i)), 1 \leq i \leq m\}$, as defined in Definition 13. Also, assume $t_1 = 0$ and $t_m = T$.*

Consider the first dimension of the estimated 0-skeleton mirror $\{\hat{\psi}_1^{(m)}(t_i), 1 \leq i \leq m\}$ from the TSG generated by this LPP with n vertices. Denote $\tilde{\tilde{\psi}}_1^{(m)}(t)$ as the piecewise linear interpolation between the points $\{(t_i, \hat{\psi}_1^{(m)}(t_i)), 1 \leq i \leq m\}$.

Then, for large n and large m , there exists a constant C and $w_m, w'_m \in \{\pm 1\}$ such that, with high probability:

$$\sup_{t \in [0, T]} |\tilde{\tilde{\psi}}_1^{(m)}(t) - w'_m \psi_0(t)| \leq C \left(\frac{m \log(n)}{\sqrt{n} \lambda_1 (-\frac{1}{2} P \mathcal{D}^{(2)} P)} + \frac{\sqrt{\sum_{i=2}^m \lambda_i^2 (-\frac{1}{2} P \mathcal{D}^{(2)} P)}}{\lambda_1 (-\frac{1}{2} P \mathcal{D}^{(2)} P)} \right) + \sup_{t \in [0, T]} |\tilde{\psi}_1^{(m)}(t) - w_m \psi_0(t)|,$$

where $\mathcal{D}^{(2)}$ is the $m \times m$ entry-wise square of the distance matrix of that mirror $\psi^{(m)}$, namely $\mathcal{D}_{ij}^{(2)} = \|\psi^{(m)}(t_i) - \psi^{(m)}(t_j)\|^2$, and $P = I - J/m$, with J being the $m \times m$ all-ones matrix. Note that $\psi^{(m)}(t_i) \in \mathbb{R}^{m-1}$ in this case.

Remark 5. Note that the mesh ρ , which originally appears in the upper bound of Theorem 5, is implicitly involved in the term $\sup_{t \in [0, T]} |\tilde{\psi}_1^{(m)}(t) - \psi_0(t)|$. In particular, when $|\tilde{\psi}_1^{(m)}(t) - \psi_0(t)| \leq \alpha_n$ for each observed time $t \in \mathcal{T}$ and both functions are L -Lipschitz, the latter quantity may be bounded above by $\alpha_n + 2L\rho$.

Also, note that we need two different $w_m, w'_m \in \{\pm 1\}$ here to account for two non-identifiability effects: one is the non-identifiability between $\hat{\psi}_1^{(m)}$ and $\psi_1^{(m)}$, and the other handles the non-identifiability between $\psi_1^{(m)}$ and ψ_0 .

The second term in parentheses is the only one which is significantly different from the upper bound in Theorem 5, and captures the distortion from approximating the asymptotically 1-d Euclidean realizable distance in \mathcal{D} with a 1-dimensional mirror.

This result leads to a similar upper bound for accuracy of the l_∞ localization estimator.

Theorem 8. *Consider an asymptotically Euclidean 1-realizable latent position process with the 0-skeleton mirror $\{\psi^{(m)}(t_i), 1 \leq i \leq m\}$ with the asymptotic mirror $\psi_0(t) = \Delta(t - t^*) I_{\{t > t^*\}}$ $t \in [0, T]$, $\Delta > 0$. Denote $\tilde{\psi}_1^{(m)}$ as the piecewise linear interpolation between the points*

$$\left\{ \left(t_i, \psi_1^{(m)}(t_i) \right), 1 \leq i \leq m \right\} \subset \mathbb{R} \times \mathbb{R}.$$

Consider the time series of networks on n vertices at points $\mathcal{T} = \{t_1, \dots, t_m\}$ with this latent position process. Assume $t_1 = 0$, $t_m = T$, and $t^* \in (t_1, t_m)$. Let $\{\hat{\psi}_1^{(m)}(t_i) | 1 \leq i \leq m\}$ denote the spectrally-derived estimated 1st dimension mirror of Athreya et al. [2022]. Let $\rho = \max_{1 \leq i < m} |t_i - t_{i+1}|$. We fit a l_∞ regression on the estimated mirror to gain the estimator. Let \hat{t} be the l_∞ localization estimator in Eq.(7), namely:

$$\hat{t}, \hat{\alpha}, \hat{\beta}_L, \hat{\beta}_R = \arg \min_{t' \in \mathcal{T}} \max_{\alpha, \beta_L, \beta_R, \beta_L \neq \beta_R} |\alpha + \beta_L(t - t') + (\beta_R - \beta_L)(t - t') I_{\{t > t'\}} - \hat{\psi}(t)|.$$

Then for large m and large n , there exists a constant C and a $w_m \in \{\pm 1\}$ such that with high probability:

$$|\hat{t} - t^*| \leq \left(\frac{Cm \log(n)}{\sqrt{n} \lambda_1(-\frac{1}{2}P\mathcal{D}^{(2)}P)} \Delta + \frac{C \sqrt{\sum_{i=2}^m \lambda_i^2(-\frac{1}{2}P\mathcal{D}^{(2)}P)}}{\lambda_1(-\frac{1}{2}P\mathcal{D}^{(2)}P)} \Delta + \frac{4 \sup_{t \in [0, T]} |\tilde{\psi}_1^{(m)}(t) - w_m \psi_0(t)|}{\Delta} + 2\rho \right) \frac{T}{\min\{T - t^*, t^*\}}.$$

Note by Definition 13, if we further assume the LPP is in-fill summably asymptotically Euclidean 1-realizable, then as $m \rightarrow \infty$, $\lambda_1(-\frac{1}{2}P\mathcal{D}^{(2)}P) \sim \Theta(m)$, $\frac{\sqrt{\sum_{i=2}^m \lambda_i^2(-\frac{1}{2}P\mathcal{D}^{(2)}P)}}{\lambda_1(-\frac{1}{2}P\mathcal{D}^{(2)}P)} \rightarrow 0$ and $\sup_{t \in [0, T]} |\tilde{\psi}_1^{(m)}(t) - w_m \psi_0(t)| \rightarrow 0$. Further if $\rho \rightarrow 0$ as $m \rightarrow \infty$ for example, $\rho = \frac{T}{m-1}$, these conditions imply consistency of the estimator \hat{t} :

Corollary 2 (Consistency of \hat{t} for in-fill summably asymptotically 1-d Euclidean realizable with piecewise linear asymptotic mirror). *When the latent position process is in-fill summably asymptotically 1-Euclidean realizable with asymptotic mirror $\psi_0(t) = \Delta(t - t^*) I_{\{t > t^*\}}$ $t \in [0, T]$, $\Delta > 0$. Consider the time series of networks on n vertices at points $\mathcal{T} = \{t_1, \dots, t_m\}$ with this latent position process. Assume $t_1 = 0$, $t_m = T$, and $t^* \in (t_1, t_m)$. Suppose that $\rho \rightarrow 0$ as $m \rightarrow \infty$. Further assume when $m \rightarrow \infty$, $\rho_m = \max_{1 \leq i \leq m-1} |t_i - t_{i+1}| \rightarrow 0$. Then for the l_∞ estimator \hat{t} defined as above, we have with high probability:*

$$|\hat{t} - t^*| \rightarrow 0 \text{ as } m \rightarrow \infty, n \rightarrow \infty.$$

Note that Model 4 satisfies the conditions in Corollary 2. The only aspect we need to address is $t_1 = \frac{1}{m} \neq 0$. This can be managed by redefining the time points as follows: for $1 \leq i \leq m$, set $t_i = \frac{i-1}{m-1}$. By employing the same argument, we can verify that this model inherits all the properties of Model 4. Essentially, this is because our mirror method focuses solely on the interpoint distances and does not concern itself with the corresponding time points. Thus, we have the corollary.

Corollary 3. *Using the l_∞ localization estimator on the observed time series of networks generated from Model 4, we can consistently localize t^* as $n \rightarrow \infty$ and $m \rightarrow \infty$.*

3.3 Numerical experiments

As we have just shown, when an LPP is asymptotically Euclidean 1-realizable, then for large n and m , the first dimension of the estimated mirror should yield good estimates for the changepoint t^* . In practice, however, there may still be useful signal contained in further MDS dimensions after the first. In the experiments of this section, we first compute the estimated mirror $\hat{\psi}$ in d dimensions, before considering the ISOMAP embedding of this curve into 1 dimension, denoted $\hat{\psi}_{d \rightarrow 1}$. This embedding retains the piecewise linear structure, but retains more of the changepoint information from other dimensions than simply embedding into 1 dimension using CMDS directly. We may write this iso-mirror as:

$$\hat{\psi}_{d \rightarrow 1}(t) = \psi_Z(t) + \epsilon_t \quad t \in [0, 1], \quad (9)$$

where ψ_Z is defined for some $t^* \in (0, 1), p, q > 0, p \neq q$ as

$$\psi_Z(t) = \begin{cases} pt & \text{for } t < t^* \\ qt + (p - q)t^* & \text{for } t \geq t^*. \end{cases}$$

Remark 6. We emphasize that two sources of error lie within the $\{\epsilon_t\}$. The first source is from finite n , since the draws from the LPP are random, as are the observed adjacency matrices A_t , the estimated distances $\min_W \|\hat{X}_t - \hat{X}_s W\|/\sqrt{n}$ will not be exactly equal to $d_{MV}(\varphi_m(t), \varphi_m(s))$. This source of error is addressed in Athreya et al. [2022]. The second source of error is from finite m , and has not been studied previously. For finite m , the first dimension of the mirror of Model 3 is not exactly ψ_Z , but does uniformly converge to ψ_Z as $m \rightarrow \infty$. This error is deterministic and small for large m compared to the random error. Moreover, since we apply ISOMAP to the mirror result, these two sources of error in the mirror estimation propagate into the iso-mirror estimate $\hat{\psi}_{d \rightarrow 1}$.

Algorithm 2 Iso-mirror estimation

- 1: Input: TSG $\{A_1, A_2, \dots, A_m\}$, ASE dimension d_1 , CMDS dimension d .
 - 2: Compute $\hat{X}_t = \text{ASE}(A_t) \in \mathbb{R}^{n \times d_1}, 1 \leq t \leq m$.
 - 3: Construct the distance matrix $\hat{\mathcal{D}} \in \mathbb{R}^{m \times m}$ where $\hat{\mathcal{D}}_{i,j} = \min_{W \in \mathcal{O}^{d_1 \times d_1}} \frac{1}{\sqrt{n}} \|\hat{X}_i - \hat{X}_j W\|_2$.
 - 4: Compute $\text{CMDS}(\hat{\mathcal{D}}) = \{\hat{\psi}(1), \hat{\psi}(2), \dots, \hat{\psi}(m)\}$, with each $\hat{\psi}(t) \in \mathbb{R}^d$.
 - 5: Apply ISOMAP on $\{\hat{\psi}(1), \hat{\psi}(2), \dots, \hat{\psi}(m)\}$ using k nearest neighbors, where k is the smallest value such that the k -nearest-neighbor graph is connected, obtaining $\{\hat{\psi}_{d \rightarrow 1}(1), \hat{\psi}_{d \rightarrow 1}(2), \dots, \hat{\psi}_{d \rightarrow 1}(m)\}$, with each $\hat{\psi}_{d \rightarrow 1}(t) \in \mathbb{R}$.
 - 6: Output: $\{\hat{\psi}_{d \rightarrow 1}(1), \hat{\psi}_{d \rightarrow 1}(2), \dots, \hat{\psi}_{d \rightarrow 1}(m)\}$.
-

As before, we wish to localize t^* from an observed TSG whose latent positions follow a random walk LPP. We set the number of vertices, n , for the graphs and generate the time series of networks comprising m graphs according to Model 4.¹ To prevent the graph from being too sparse, we choose the starting point as $c = 0.1$, resulting in $\delta = \frac{0.9}{m}$. The t^* is always set to be $1/2$ and we always select an even number for m from the set $16, 24, 32, 40$. We then set $p = 0.4$ and $q = 0.3$.

For fixed values of $n, m, p = 0.4, q = 0.3$, and $t_m^* = \frac{m}{2}$, we generate a time series of graphs as follows: We start with a vector $X_0 \in \mathbb{R}^{n \times 1}$, with all entries set to 0.1 , representing the starting point for the n latent positions. For subsequent time points, we independently draw n samples from $\text{Bernoulli}(p)$. The i th entry of $(X_t)_i = (X_{t-1})_i$ if $u_i = 0$, or $(X_t)_i = (X_{t-1})_i + \frac{0.9}{m}$ if $u_i = 1$. This process repeats until $X_{\frac{m}{2}}$ is reached. For $X_{\frac{m}{2}+1}$, we switch the jump probability to $q = 0.3$. Eventually, we obtain $\{X_1, \dots, X_m\}$ as the realized latent position matrices for n vertices. Then for each time, we generate an RDPG using the latent positions in X_t , obtaining a TSG $\{A_1, \dots, A_m\}$ as defined in Definition 6.

For the estimation, we set the ASE embedding dimension to $d_1 = 1$, and consider various values of the CMDS embedding dimension d . Applying our Spectral MIRROR procedure to $\{A_1, \dots, A_m\}$ as in Algorithm 2, we obtain the iso-mirror estimate $\hat{\psi}_{d \rightarrow 1}$. We then compute the l_∞ localization estimator for the changepoint, following Algorithm 1. In this algorithm, the optimization problem at step 3 is reformulated as a constrained linear programming problem, which we solve using the `lpSolveAPI`² function in R. This procedure is repeated for each Monte Carlo simulation, with each iteration yielding \hat{t}_{mc} .

To evaluate the performance of our estimator, we consider the squared error $(\hat{t}_{mc} - t^*)^2$ for each iteration. We run the Monte Carlo simulation $nmc = 2000$ times, and record the mean of these 2000 realizations as the mean square error (MSE):

$$\text{MSE} := \frac{1}{nmc} \sum_{mc=1}^{nmc} (\hat{t}_{mc} - t^*)^2.$$

¹All of our codes are available: <https://github.com/TianyiChen97/Euclidean-mirrors-and-first-order-changepoints-in-network-time-series>

²<https://cran.r-project.org/web/packages/lpSolveAPI/index.html>

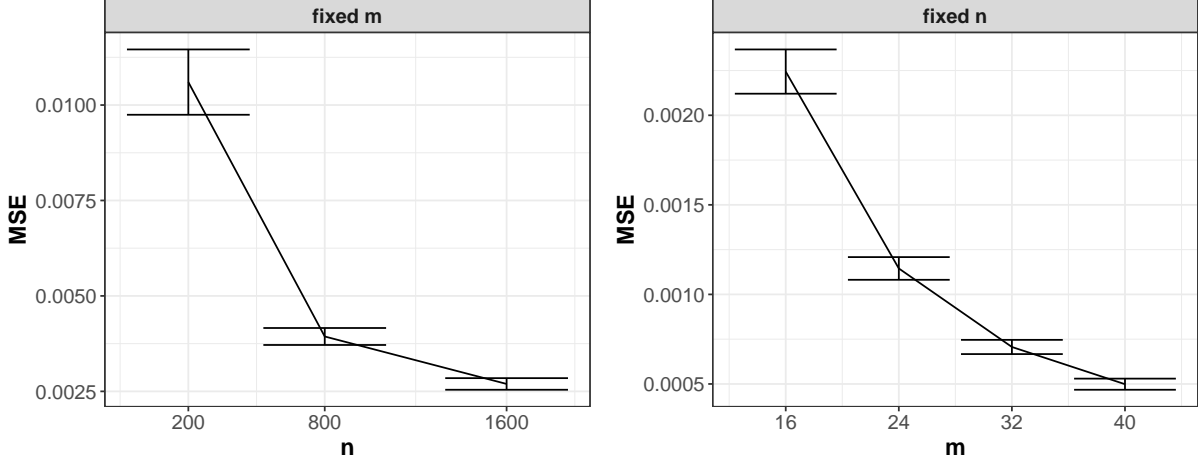


Figure 5: Accuracy of network changepoint estimator \hat{t} as a function of m and n when using the 1st dimension of the estimated mirror. $p = 0.4$, $q = 0.3$, $|p - q| = 0.1$, $nmc = 2000$ and $t^* = \frac{1}{2}$ fixed for both figures. Left: $m = 12$ fixed. Right: $n = 800$ fixed. We see the MSE tends to 0 for fixed $n = 800$ with m growing and for fixed $m = 12$ with n growing.

Next, we calculate the sample standard deviation for the 2000 realizations:

$$\text{std} := \sqrt{\frac{1}{nmc - 1} \sum_{mc=1}^{nmc} \left((\hat{t}_{mc} - t^*)^2 - \text{MSE} \right)^2}.$$

Using the normal approximation, we can construct the confidence interval for the MSE as:

$$\text{CI} = \text{MSE} \pm \frac{1.96}{\sqrt{nmc}} \times \text{std},$$

and we plot the CI in Figures 5 and 6.

In the first setting we fix CMDS embedding dimension $d = 1$ and $p = 0.4$, $q = 0.3$. Note when $d = 1$, applying ISOMAP to the CMDS mirror makes no difference, so we may skip this step. We consider fixed $n = 800$ and vary m over 16, 24, 32, 40. Next, we fix $m = 12$ and vary n over 200, 800, 1600. These results can be seen in Figure 5. For fixed m , MSE drops quickly with increasing n . For fixed $n = 800$, we also see bigger m has significantly smaller MSE.

Now we fix $|p - q| = 0.1$ and see accuracy of \hat{t} when iso-mirror uses different MDS embedding dimension. In Fig 6 we see the phenomenon that by going into deeper dimensions, the MSE first goes down and then goes up again. Recall in our model, deep dimensions still have signals for changepoint thus not using deeper dimensions will cause signal loose, that is, introducing bias. Meanwhile embedding in deeper dimensions will also introduce more variance. Thus the “V” shape phenomenon in MSE is a phenomenon of bias-variance trade-off. Comparing left two panels and right two panels, we see as n increases, the variance drops dramatically, so the estimator can benefit from going into deeper dimension. Comparing the upper two panels and the lower two panels, we see the benefits of going into deeper dimensions gets smaller. This is because as m gets larger, there are less signals in the deeper dimension.

3.4 Real data example: organoid

In this section we study a real data case where we apply our spectral MIRROR method on a time series of brain organoid connectomes. The brain organoids we consider are self-organizing structures composed of

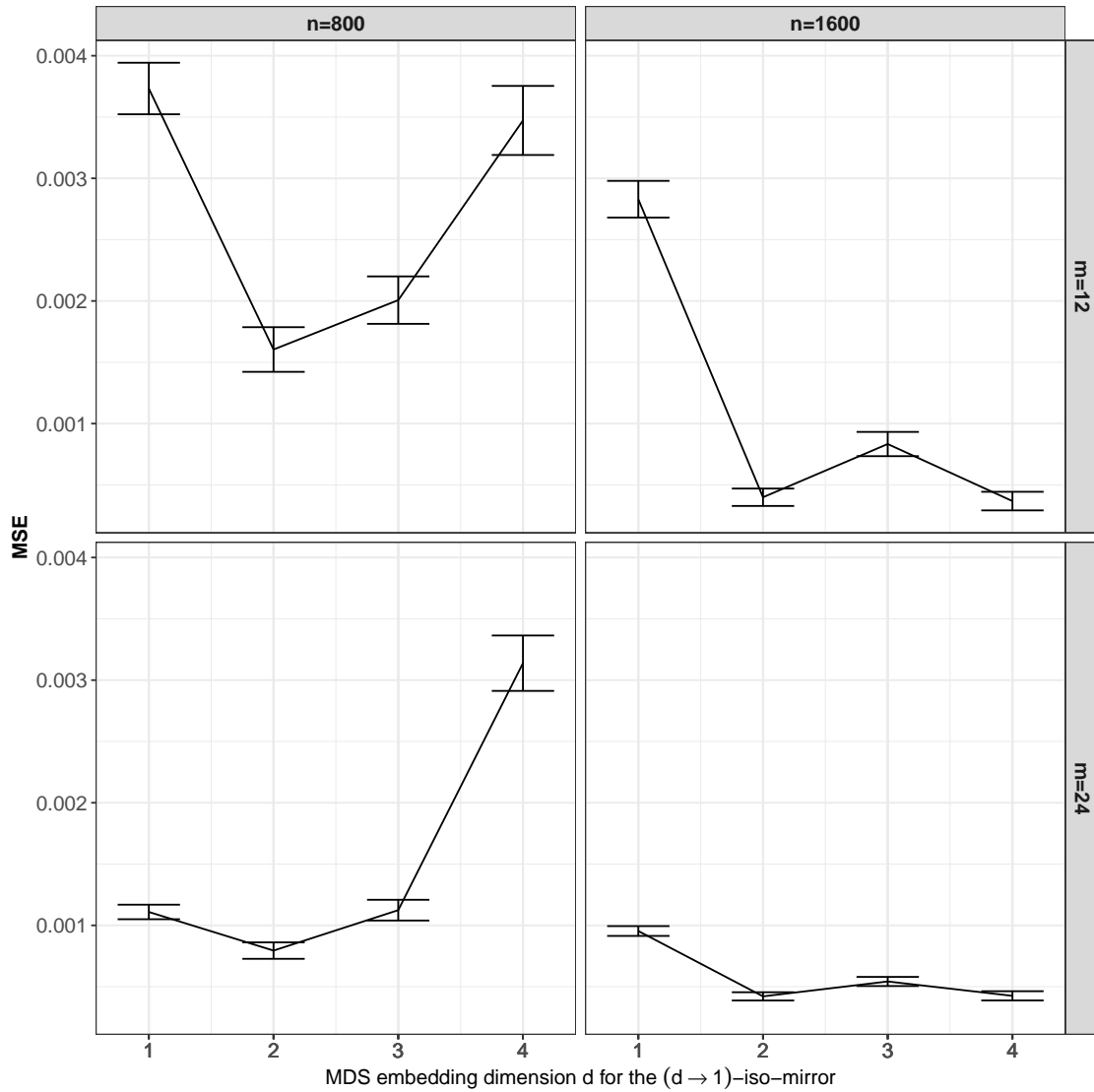


Figure 6: Accuracy of network changepoint estimator \hat{t} as a function of MDS embedding dimension d when using the $(d \rightarrow 1)$ -iso-mirror $\hat{\psi}_{d \rightarrow 1}$. Upper left: $n = 800, m = 12$. Upper right: $n = 1600, m = 12$. Lower left: $n = 800, m = 24$. Lower right: $n = 1600, m = 24$. In all cases, $p = 0.4, q = 0.3, t^* = \frac{1}{2}$ and $nmc = 2000$. Comparing left two panels and right two panels, we see as n increases, the l_∞ estimator can benefit from going into deeper dimension. Comparing the upper two panels and the lower two panels, we see the benefits of going into deeper dimensions gets smaller. This is because as m gets larger, there are less signals in the deeper dimension.

roughly 2.5 million neural cells. They are generated from human induced pluripotent stem cells (hiPSCs) Muguruma et al. [2015]. After growing for 6 weeks, they are plated in 8 wells of a multi-electrode array (MEA) plate (Axion Biosystem, Atlanta, GA, USA). MEA contains 64 low-impedance (0.04 MU) platinum microelectrodes with 30 μm of diameter spaced by 200 μm . Each well contains two or three organoids. Then, to characterize the functional development of the organoids, extracellular spontaneous electrical activity is recorded weekly using Maestro MEA system and AxIS Software Spontaneous Neural Configuration (Axion Biosystems) with a 0.1-Hz to 5-kHz band-pass filter. Spikes are detected with an adaptive threshold crossing set to 5.5 times the standard deviation of the estimated noise for each electrode. Each time series consists of five minutes of recorded neural activity across 10 months and the data are recorded irregularly – not exactly once a week. A combination of principal component analysis and k-means clustering is used to spike sort the multi-unit activity from the 64 electrodes of each well. To approximate the functional connections between neurons, the algorithm proposed in Puppo et al. [2021] is applied and we force the accepted degree of temporal approximation to be 0.

In the end, for well 34, 38 functional connectivity networks on 181 vertices across 246 days are obtained. This is our time series of organoid networks. Since the alignment of vertices among the networks is unknown, we apply the Fast Approximate Quadratic algorithm Vogelstein et al. [2015] to perform graph matching on all the networks. We avoid the birth and death period and choose only 30 graphs so $m = 30$. After that, we find the largest common connected component among the aligned networks, which contains $n = 44$ nodes. Then, we compute the estimated iso-mirror following Algorithm 1. Finally, we fit the data with l_∞ regression, pre-specifying only 1 changepoint. This changepoint is estimated to occur on day 156 (see Figure 7). On the right panel, we also plot the control chart, which is simply the Frobenius norm difference between the adjacency matrices of two consecutive time points. Notably, this Frobenius norm difference consistently deviates from zero across almost all pairs of consecutive points. This pattern indicates that the time series of functional connectivity networks is in a state of constant flux. As a result, it is unrealistic to apply the zeroth-order changepoint model 1 to this real-world data scenario. Such a situation would likely render most network changepoint detection algorithms ineffective. Our proposed method, however, constructs a distance matrix and applies CMDS and ISOMAP to obtain a 1d Euclidean embedding, the iso-mirror, that takes into account all time stamps and the global dynamics of the time series of networks as opposed to considering pairwise differences, which is only a local property. The piecewise linearity exhibited in the iso-mirror then motivates us to use the l_∞ estimator to localize the changepoint.

4 Conclusion and Discussion

Changepoint localization for network time series is a key problem in joint network inference, complicated by the fact that a changepoint can be more delicate than a simple shift in network distribution. For latent position process networks, we address three core points in this work: we formalize the concept of changepoints of different orders; we construct, in Model 3, a time series of latent position networks with a first-order changepoint; and we show that such a changepoint can be successfully localized through spectral decompositions of network observations and spectrally-derived estimates of the associated Euclidean mirror. Building on work in Athreya et al. [2022], we also define asymptotic Euclidean realizability for a network time series, highlighting the significance of both network size n and the number of sampled time points m in such a time series.

Because the Euclidean mirror uses classical multidimensional scaling to represent a covariance-related dissimilarity measure for latent position networks, two natural questions arise: what is the impact of the choice of dissimilarity, and what is the appropriate embedding dimension in CMDS? In our simulations, we underscore the efficacy of our mirror-based changepoint localization for Model 3 and also illustrate the bias-variance trade-off governed by this choice of embedding dimension. Our real data analysis of brain organoid networks exhibits an approximate piecewise linear mirror structure for our covariance-based network dissimilarity, and here again, our algorithm effectively locates a biologically relevant changepoint.

Ongoing work encompasses several theoretical issues. First, a sharper upper bound in Theorem 6, which requires improved distributional results on $\hat{\psi} - \psi$; second, a localization estimate obtained with respect to

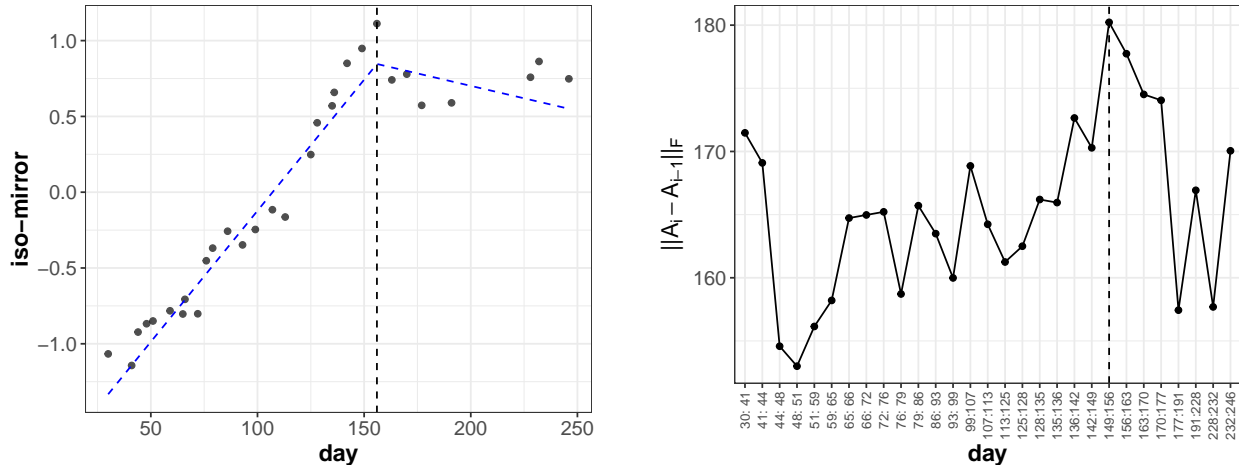


Figure 7: Real data example with time series of approximate functional connectivity graphs. On the left panel is iso-mirror result. The black dots are the estimated iso-mirror. The dashed blue piecewise linear curve is l_∞ regression fit, with the vertical line as the estimated changepoint at day 156. On the right panel is the control chart for pairwise Frobenius norm difference for the graphs. It also shows $\|A_{156} - A_{149}\|_F$ is the maximum. However the chart indicates the time series of networks are constantly changing and the underlying dynamic of the networks cannot be described as a zeroth-order changepoint model, which renders most changepoint algorithms based on such an assumption ineffective.

different norms than the current l_∞ norm, in which stronger convexity properties of a chosen norm may lead to performance gains when the graph size n is fixed or grows more slowly relative to the sample size m of networks; third, a deeper exploration of the effects of ISOMAP on the mirror estimate, particularly its impact on aggregating the errors between the estimated and true mirror; fourth, understanding Euclidean realizability for dimensions $c > 1$, including the construction of an exactly c -realizable process for $c > 1$ and the bias-variance tradeoff in estimation as a function of CMDS embedding dimension. Finally, this paper is dedicated to localization, but detection is, of course, a critical related task. An intuitive starting point is to use $|\hat{\beta}_R - \hat{\beta}_L|$ as the test statistic. Determining the asymptotic distribution of this test statistic mandates a deeper understanding of the error term $\epsilon_t = \hat{\psi}_{d \rightarrow 1}(t) - \psi_Z(t)$ in (9). Furthermore, expanding this work to detect an indeterminate number of changepoints, followed by their subsequent localization, requires a more efficient algorithm than the current grid search we employ. The success of mirror-based estimation for simple latent position networks and the associated provable guarantees for localization suggest that these techniques have wider promise in the analysis of evolving networks.

References

- Joshua Agterberg, Zachary Lubbets, and Jesús Arroyo. Joint spectral clustering in multilayer degree-corrected stochastic blockmodels. *arXiv preprint arXiv:2212.05053*, 2022.
- Avanti Athreya, Zachary Lubbets, Youngser Park, and Carey E Priebe. Discovering underlying dynamics in time series of networks. *arXiv preprint arXiv:2205.06877*, 2022.
- Monika Bhattacharjee, Moulinath Banerjee, and George Michailidis. Change point estimation in a dynamic stochastic block model. *Journal of machine learning research*, 21(107):1–59, 2020.
- George EP Box, Gwilym M Jenkins, Gregory C Reinsel, and Greta M Ljung. *Time series analysis: forecasting and control*. John Wiley & Sons, 2015.

- Joshua Cape, Minh Tang, and Carey E Priebe. The two-to-infinity norm and singular subspace geometry with applications to high-dimensional statistics. *Annual of Statistics*, 2019.
- Tianyi Chen, Youngser Park, Ali Saad-Eldin, Zachary Lubbets, Avanti Athreya, Benjamin D Pedigo, Joshua T Vogelstein, Francesca Puppo, Gabriel A Silva, Alysson R Muotri, et al. Discovering a change point and piecewise linear structure in a time series of organoid networks via the iso-mirror. *Applied Network Science*, 8(1):45, 2023.
- Persi Diaconis, Sharad Goel, and Susan Holmes. Horseshoes in multidimensional scaling and local kernel methods. *The Annals of Applied Statistics*, 2(3):777–807, 2008.
- Xing Fan, Marianna Pensky, Feng Yu, and Teng Zhang. Alma: Alternating minimization algorithm for clustering mixture multilayer network. *Journal of Machine Learning Research*, 23(330):1–46, 2022.
- Bing-Yi Jing, Ting Li, Zhongyuan Lyu, and Dong Xia. Community detection on mixture multilayer networks via regularized tensor decomposition. *The Annals of Statistics*, 49(6):3181–3205, 2021.
- Andrew Jones and Patrick Rubin-Delanchy. The multilayer random dot product graph. *arXiv preprint arXiv:2007.10455*, 2020.
- Benjamin Kedem and Konstantinos Fokianos. *Regression models for time series analysis*. John Wiley & Sons, 2005.
- Yik Lun Kei, Jialiang Li, Hangjian Li, Yanzhen Chen, and Oscar Hernan Madrid Padilla. Change point detection in dynamic graphs with generative model. *arXiv preprint arXiv:2404.04719*, 2024.
- Peter W MacDonald, Elizaveta Levina, and Ji Zhu. Latent space models for multiplex networks with shared structure. *Biometrika*, 109(3):683–706, 2022.
- Keiko Muguruma, Ayaka Nishiyama, Hideshi Kawakami, Kouichi Hashimoto, and Yoshiki Sasai. Self-organization of polarized cerebellar tissue in 3d culture of human pluripotent stem cells. *Cell reports*, 10(4):537–550, 2015.
- Oscar Hernan Madrid Padilla, Yi Yu, Daren Wang, and Alessandro Rinaldo. Optimal nonparametric multivariate change point detection and localization. *IEEE Transactions on Information Theory*, 68(3):1922–1944, 2021.
- Oscar Hernan Madrid Padilla, Yi Yu, and Carey E Priebe. Change point localization in dependent dynamic nonparametric random dot product graphs. *The Journal of Machine Learning Research*, 23(1):10661–10719, 2022.
- Konstantinos Pantazis, Avanti Athreya, Jesús Arroyo, William N Frost, Evan S Hill, and Vince Lyzinski. The importance of being correlated: Implications of dependence in joint spectral inference across multiple networks. *Journal of Machine Learning Research*, 23(141):1–77, 2022.
- S. Paul and Y. Chen. Spectral and matrix factorization methods for consistent community detection in multi-layer networks. *The Annals of Statistics*, 48(1):230–250, 2020.
- Francesca Puppo, Deborah Pré, Anne G Bang, and Gabriel A Silva. Super-selective reconstruction of causal and direct connectivity with application to in vitro ipsc neuronal networks. *Frontiers in Neuroscience*, 15: 647877, 2021.
- Robert H Shumway, David S Stoffer, and David S Stoffer. *Time series analysis and its applications*, volume 3. Springer, 2000.
- D. L. Sussman, M. Tang, D. E. Fishkind, and C. E. Priebe. A consistent adjacency spectral embedding for stochastic blockmodel graphs. *Journal of the American Statistical Association*, 107:1119–1128, 2012.

- M. Tang, D. L. Sussman, and C. E. Priebe. Universally consistent vertex classification for latent position graphs. *Annals of Statistics*, 41:1406 – 1430, 2013.
- Joshua B Tenenbaum, Vin de Silva, and John C Langford. A global geometric framework for nonlinear dimensionality reduction. *Science*, 290(5500):2319–2323, 2000.
- Michael W Trosset and Gokcen Buyukbas. Rehabilitating isomap: euclidean representation of geodesic structure. *arXiv preprint arXiv:2006.10858*, 2020.
- Nicolas Verzelen, Magalie Fromont, Matthieu Lerasle, and Patricia Reynaud-Bouret. Optimal change-point detection and localization. *The Annals of Statistics*, 51(4):1586–1610, 2023.
- Joshua T Vogelstein, John M Conroy, Vince Lyzinski, Louis J Podrazik, Steven G Kratzer, Eric T Harley, Donniell E Fishkind, R Jacob Vogelstein, and Carey E Priebe. Fast approximate quadratic programming for graph matching. *PLoS One*, 10(4):e0121002, April 2015. URL <http://dx.doi.org/10.1371/journal.pone.0121002>.
- Daren Wang, Yi Yu, and Alessandro Rinaldo. Optimal change point detection and localization in sparse dynamic networks. *arXiv e-prints*, 2021.
- Fan Wang, Wanshan Li, Oscar Hernan Madrid Padilla, Yi Yu, and Alessandro Rinaldo. Multilayer random dot product graphs: Estimation and online change point detection. *arXiv preprint arXiv:2306.15286*, 2023.
- P. J. Wolfe and S. C. Olhede. Nonparametric graphon estimation. *arXiv preprint arXiv: 1309.5936*, 2013.
- Mu Zhu and Ali Ghodsi. Automatic dimensionality selection from the scree plot via the use of profile likelihood. *Computational Statistics & Data Analysis*, 51(2):918–930, 2006.
- Tiona Zuzul, Emily Cox Pahnke, Jonathan Larson, Patrick Bourke, Nicholas Caurvina, Neha Parikh Shah, Fereshteh Amini, Jeffrey Weston, Youngser Park, Joshua Vogelstein, et al. Dynamic silos: Increased modularity in intra-organizational communication networks during the covid-19 pandemic. *arXiv preprint arXiv:2104.00641*, 2021.

5 Appendix

5.1 Proof of Lemma 1

Proof. Suppose $t' < t$ and $t, t' \in \{1, 2, \dots, n\}$ and $a := t - t'$. Since X_t is a one-dimensional random variable,

$$\begin{aligned} d_{MV}(X_t, X_{t'})^2 &= \min_W \|\mathbb{E}[(X_t - WX_{t'})(X_t - WX_{t'})^\top]\|_2 \\ &= \min_W |\mathbb{E}[X_t^2 - 2WX_tX_{t'} + W^2X_{t'}^2]|. \end{aligned}$$

To address the minimization over orthogonal matrices, observe that in one dimension, the only orthogonal transformations correspond to multiplication by 1 or -1 . So we need only consider the two cases $W = 1$ or $W = -1$. Since $X_t \geq 0$ for all t , $\mathbb{E}[X_tX_{t'}] \geq 0$. Thus $W = 1$ minimizes the above, and we conclude that

$$d_{MV}(X_t, X_{t'})^2 = \mathbb{E}[(X_t - X_{t'})^2].$$

Notice that the increment $X_t - X_{t'}$ satisfies $X_t - X_{t'} = V_a\delta$, where $V_a \sim \text{Binomial}(a, p)$. Thus

$$\begin{aligned} \mathbb{E}[(X_t - X_{t'})^2] &= \delta^2\mathbb{E}[V_a^2] \\ &= (a^2p^2 + a(p - p^2))\delta^2. \end{aligned}$$

□

5.2 Proof of Lemma 4

Proof. Fix $\beta \in [0, 1]$. Put $t_{\beta, m} = \lfloor m\beta \rfloor$. Then $X_{t_{\beta, m}}^{(m)} = \frac{V_{t_{\beta, m}}}{m}$, where $V_{t_{\beta, m}}$ is a Binomial random variable with $t_{\beta, m}$ trials and success probability p . Thus $\mathbb{E}[X_{t_{\beta, m}}^{(m)}] = \frac{\lfloor m\beta \rfloor p}{m}$ and as $m \rightarrow \infty$,

$$\mathbb{E}[X_{t_{\beta, m}}^{(m)} - \beta p]^2 = \mathbb{E}[X_{t_{\beta, m}}^{(m)} - \mathbb{E}[X_{t_{\beta, m}}^{(m)}] + \mathbb{E}[X_{t_{\beta, m}}^{(m)}] - \beta p]^2 = \frac{\lfloor m\beta \rfloor p(1-p)}{m^2} + \left(\frac{\lfloor m\beta \rfloor p}{m} - \beta p\right)^2 \rightarrow 0.$$

Thus $X_{t_{\beta, m}}^{(m)} \xrightarrow{L^2} \beta p = Z_\beta$.

□

5.3 Proof of Lemma 3

Proof. When $\varphi(t)$ is deterministic, for any x, y :

$$\begin{aligned} d_{MV}(\varphi(x), \varphi(y))^2 &= \min_{W \in \mathcal{O}^{d \times d}} \|\mathbb{E}[(\varphi(x) - W\varphi(y))(\varphi(x) - W\varphi(y))^\top]\|_2^2 \\ &= \min_{W \in \mathcal{O}^{d \times d}} \|(\varphi(x) - W\varphi(y))(\varphi(x) - W\varphi(y))^\top\|_2 \\ &= \min_{W \in \mathcal{O}^{d \times d}} \|\varphi(x) - W\varphi(y)\|_2^2 \\ &= (\|\varphi(x)\|_2 - \|\varphi(y)\|_2)^2. \end{aligned}$$

The last equality follows since $\|\varphi(x) - W\varphi(y)\|_2^2 \geq (\|\varphi(x)\|_2 - \|\varphi(y)\|_2)^2$ always holds and there exists a W such that $\varphi(x)$ and $\varphi(y)$ are linearly dependent, in which case the lower bound is achieved. After centering the mirror we get the result. □

5.4 Proof of Theorem 2

Proof. First let's state some properties of the two distance matrices $\mathcal{D}_{\varphi_m}^{(2)}$ and $\mathcal{D}_Z^{(2)}$. Denote the eigenvalues and the corresponding orthonormal eigenvectors of $-\frac{1}{2}P\mathcal{D}_Z^{(2)}P$ and $-\frac{1}{2}P\mathcal{D}_{\varphi_m}^{(2)}P$ respectively as $\lambda_1, \lambda_2, \dots, \lambda_m$ and U_1, U_2, \dots, U_m ; $\tilde{\lambda}_1, \tilde{\lambda}_2, \dots, \tilde{\lambda}_m$ and $\tilde{U}_1, \tilde{U}_2, \dots, \tilde{U}_m$. Then the k th dimension of the mirror for Model 3 is: $\sqrt{\tilde{\lambda}_k}\tilde{U}_k$. Since $\mathcal{D}_Z^{(2)}$ is exactly Euclidean 1-realizable, its mirror is $\sqrt{\lambda_1}U_1$.

Property 1. $\lambda_1 \sim \Theta(m)$, $\lambda_i = 0$ for $i \geq 2$. And $\|U_1\|_{2 \rightarrow \infty} \sim O(\frac{1}{\sqrt{m}})$. For $A \in \mathbb{R}^{p_1 \times p_2}$, $\|A\|_{2 \rightarrow \infty}$ is the maximum Euclidean row norm of A .

Proof. Since $\mathcal{D}_Z^{(2)}$ is exactly 1-d Euclidean realizable with mirror $\sqrt{\lambda_1}U_1$, $-\frac{1}{2}P\mathcal{D}_Z^{(2)}P = \lambda_1 U_1 U_1^\top$ where $\sqrt{\lambda_1}U_1 = (\psi_Z(\frac{1}{m}), \psi_Z(\frac{2}{m}), \dots, \psi_Z(\frac{m}{m}))^\top$. Thus

$$\frac{\lambda_1}{m} = \frac{\sum_{i=1}^m \psi_Z^2(\frac{i}{m})}{m} \rightarrow \int_0^1 \psi_Z^2(x) dx = C \text{ as } m \rightarrow \infty.$$

That is, $\lambda_1 \sim \Theta(m)$. What's more, since

$$\|\sqrt{\lambda_1}U_1\|_{2 \rightarrow \infty} = \left\| \left(\psi_Z\left(\frac{1}{m}\right), \psi_Z\left(\frac{2}{m}\right), \dots, \psi_Z\left(\frac{m}{m}\right) \right)^\top \right\|_{2 \rightarrow \infty} \leq \max_{t \in [0,1]} |\psi_Z(t)| \leq p + q + c_0,$$

thus $\|U_1\|_{2 \rightarrow \infty} \sim O(\frac{1}{\sqrt{m}})$. \square

Property 2. $\tilde{\lambda}_1 \sim \Theta(m)$, $\tilde{\lambda}_i \sim O(1)$ for $i \geq 2$, and $\|\mathcal{D}_{\varphi_m}^{(2)} - \mathcal{D}_Z^{(2)}\|_\infty \sim O(1)$. For $A \in \mathbb{R}^{p_1 \times p_2}$ $\|A\|_\infty$ is the maximum absolute row sum of A .

Proof. Because we have $(\mathcal{D}_{\varphi_m}^{(2)} - \mathcal{D}_Z^{(2)})_{i,j} \sim O(\frac{1}{m})$ hold for all i, j , so $\|\mathcal{D}_{\varphi_m}^{(2)} - \mathcal{D}_Z^{(2)}\|_\infty \sim O(1)$. Also note $\|P\|_2 = 1$, so

$$\left\| \frac{1}{2}P(\mathcal{D}_{\varphi_m}^{(2)} - \mathcal{D}_Z^{(2)})P \right\|_F^2 \leq \left\| \frac{1}{2}(\mathcal{D}_{\varphi_m}^{(2)} - \mathcal{D}_Z^{(2)}) \right\|_F^2 \|P\|_2^4 = \left\| \frac{1}{2}(\mathcal{D}_{\varphi_m}^{(2)} - \mathcal{D}_Z^{(2)}) \right\|_F^2 \sim O(1),$$

and $\frac{1}{2}P(\mathcal{D}_{\varphi_m}^{(2)} - \mathcal{D}_Z^{(2)})P$ is Hermitian. Thus

$$\left| \lambda_1 \left(\frac{1}{2}P(\mathcal{D}_{\varphi_m}^{(2)} - \mathcal{D}_Z^{(2)})P \right) \right| \leq \sum_{i=1}^m \left| \lambda_i \left(\frac{1}{2}P(\mathcal{D}_{\varphi_m}^{(2)} - \mathcal{D}_Z^{(2)})P \right) \right|^2 = \left\| \frac{1}{2}P(\mathcal{D}_{\varphi_m}^{(2)} - \mathcal{D}_Z^{(2)})P \right\|_F^2 \sim O(1).$$

Thus $\left| \lambda_1 \left(\frac{1}{2}P(\mathcal{D}_{\varphi_m}^{(2)} - \mathcal{D}_Z^{(2)})P \right) \right| \sim O(1)$. Then by Weyl's theorem, since $\lambda_1 \sim \Theta(m)$ and $\lambda_i = 0$ for $i \geq 2$, we have the results. \square

Property 3. $\|\sqrt{\tilde{\lambda}_1}\tilde{U}_1 - \sqrt{\lambda_1}U_1\|_{2 \rightarrow \infty} \rightarrow 0$ as $m \rightarrow \infty$.

Proof. From Property 1, we know $\lambda_1 \sim \Theta(m)$ and $\|U_1\|_{2 \rightarrow \infty} \sim O(\frac{1}{\sqrt{m}})$. Then there exists a $w = 1$ or $w = -1$ such that:

$$\begin{aligned} \|\sqrt{\tilde{\lambda}_1}\tilde{U}_1 - w\sqrt{\lambda_1}U_1\|_{2 \rightarrow \infty} &\leq \sqrt{\tilde{\lambda}_1}\|\tilde{U}_1 - wU_1\|_{2 \rightarrow \infty} + \left(|\sqrt{\tilde{\lambda}_1} - w\sqrt{\lambda_1}| \|U_1\|_{2 \rightarrow \infty} \right) \\ &\leq \left(\frac{c\sqrt{\tilde{\lambda}_1}\|\frac{1}{2}P(\mathcal{D}_{\varphi_m}^{(2)} - \mathcal{D}_Z^{(2)})P\|_\infty}{\lambda_1} + |\sqrt{\tilde{\lambda}_1} - w\sqrt{\lambda_1}| \right) \|U_1\|_{2 \rightarrow \infty}. \end{aligned}$$

The last inequality is Theorem 4.2 in Cape et al. [2019], which we quote here:

Theorem 9. Let $X, E \in \mathbb{R}^{p \times p}$ be symmetric matrices where $\text{rank}(X) = r$ and X has spectral decomposition $X = U\Lambda U^T + U_\perp\Lambda_\perp U_\perp^T = U\tilde{\Lambda}U^T$ with leading eigenvalues $|\lambda_1| \geq |\lambda_2| \geq \dots \geq |\lambda_r| \geq 0$. If $|\lambda_r| \geq 4\|E\|_\infty$, then there exists an orthogonal matrix $W_U \in O_r$ such that

$$\|\tilde{U} - UW_U\|_{2 \rightarrow \infty} \leq \frac{14}{3} \left(\frac{\|E\|_\infty}{|\lambda_r|} \right) \|U\|_{2 \rightarrow \infty}.$$

The condition that $|\lambda_1| > 4\|P(\mathcal{D}_{\varphi_m}^{(2)} - \mathcal{D}_Z^{(2)})P\|_\infty$ is satisfied since $\lambda_1 \sim \Theta(m)$ while $\|P(\mathcal{D}_{\varphi_m}^{(2)} - \mathcal{D}_Z^{(2)})P\|_\infty \leq \|\mathcal{D}_{\varphi_m}^{(2)} - \mathcal{D}_Z^{(2)}\|_\infty \|P\|_\infty^2 \leq 4\|\mathcal{D}_{\varphi_m}^{(2)} - \mathcal{D}_Z^{(2)}\|_\infty \sim O(1)$.

Now we consider $|\sqrt{\tilde{\lambda}_1} - \sqrt{\lambda_1}|$. Note $|\sqrt{\tilde{\lambda}_1} - \sqrt{\lambda_1}| = \frac{|\tilde{\lambda}_1 - \lambda_1|}{\sqrt{\tilde{\lambda}_1 + \sqrt{\lambda_1}}} \leq \frac{O(1)}{\Theta(\sqrt{m})} \sim O\left(\frac{1}{\sqrt{m}}\right)$. Thus there exists a constant C such that $|\sqrt{\tilde{\lambda}_1} - \sqrt{\lambda_1}| \leq \frac{C}{\sqrt{m}}$, So the above can be further bounded by:

$$\left(\frac{\left(\sqrt{\lambda_1} + \frac{C}{\sqrt{m}}\right) \|\frac{1}{2}P(\mathcal{D}_{\varphi_m}^{(2)} - \mathcal{D}_Z^{(2)})P\|_\infty}{\lambda_1} + |\sqrt{\tilde{\lambda}_1} - \sqrt{\lambda_1}| \right) \|U_1\|_{2 \rightarrow \infty},$$

which is of order $\frac{1}{m}$ and we get the desired result. \square

Property 4. $\frac{\sum_{i=2}^m \tilde{\lambda}_i^2}{\lambda_1^2} \rightarrow 0$ as $m \rightarrow \infty$.

Proof. By Hoffman-Wielandt inequality:

$$\sum_{i=2}^m (\tilde{\lambda}_i - \lambda_i)^2 \leq \left\| \frac{1}{2}P(\mathcal{D}_Z^{(2)} - \mathcal{D}_{\varphi_m}^{(2)})P \right\|_F^2 \sim O(1).$$

Note $\lambda_i = 0$ for $i \geq 2$. Thus we have

$$\sum_{i=2}^m \tilde{\lambda}_i^2 \sim O(1),$$

Recall from Property 2 $\tilde{\lambda}_1 \sim \Theta(m)$, then the result follows. \square

Now we prove the 4 claims of Theorem 2. Note that (2) is immediate because

$$\max_{i,j \in \{1,2,\dots,m\}} \left| \left(\mathcal{D}_{\varphi_m}^{(2)} - \mathcal{D}_Z^{(2)} \right)_{i,j} \right| \leq \frac{1}{4m}$$

for any m . (3) and (4) are proved in Property 2 and 4.

For (1), recall our model 3 is a discrete time LPP with finite m , so $\tilde{\psi}_1^{(m)}$ is the piecewise linear interpolation between the points $\left\{ \left(t_i, \left(\sqrt{\tilde{\lambda}_1} \tilde{U}_1 \right)_i \right), 1 \leq i \leq m \right\}$, and define $\tilde{\psi}_1^{(m)}$ on $[0, t_1]$ so that it is linear on $[0, t_2]$. Also we denote $\tilde{\psi}_Z$ as the piecewise linear interpolation between the points $\left\{ \left(t_i, \left(\sqrt{\lambda_1} U_1 \right)_i \right), 1 \leq i \leq m \right\} = \left\{ \left(t_i, \psi_Z \left(\frac{i}{m} \right) \right), 1 \leq i \leq m \right\}$. Then

$$\sup_{t \in [0,1]} |\tilde{\psi}_1^{(m)}(t) - \psi_Z(t)| \leq \sup_{t \in [0,1]} |\tilde{\psi}_1^{(m)}(t) - \tilde{\psi}_Z(t)| + \sup_{t \in [0,1]} |\tilde{\psi}_Z(t) - \psi_Z(t)|.$$

Note since $\tilde{\psi}_1^{(m)}(t)$ and $\tilde{\psi}_Z$ are the piecewise linear interpolation at the same time points $\{t_1, t_2, \dots, t_m\}$. Thus

$$\sup_{t \in [0,1]} |\tilde{\psi}_1^{(m)}(t) - \tilde{\psi}_Z(t)| = \max_{t \in \{0, t_1, t_2, \dots, t_m\}} |\tilde{\psi}_1^{(m)}(t) - \tilde{\psi}_Z(t)| \leq 3 \|\sqrt{\tilde{\lambda}_1} \tilde{U}_1 - \sqrt{\lambda_1} U_1\|_{2 \rightarrow \infty} \rightarrow 0,$$

because of Lemma 5, Property 3, and $|\tilde{\psi}_1^{(m)}(0) - \tilde{\psi}_Z(0)| \leq 3 \max_{t \in \{t_1, t_2\}} |\tilde{\psi}_1^{(m)}(t) - \tilde{\psi}_Z(t)|$. The third point follows from the linearity on $[0, t_2]$.

Now consider $\sup_{t \in [0,1]} |\tilde{\psi}_Z(t) - \psi_Z(t)|$. Recall $\tilde{\psi}_Z(t) = \psi_Z(t)$ for $t \in \{t_1, t_2, \dots, t_m\}$ and both of them are piecewise linear. Then $\sup_{t \in [0,1]} |\tilde{\psi}_Z(t) - \psi_Z(t)| > 0$ only if $t^* \notin \{t_1, t_2, \dots, t_m\}$. When $t^* \notin \{t_1, t_2, \dots, t_m\}$, $\tilde{\psi}_Z$ and ψ_Z disagree only on the interval $[t_i, t_{i+1}]$ containing t^* . We can bound the difference by

$$\sup_{t \in [0,1]} |\tilde{\psi}_Z(t) - \psi_Z(t)| = \left| \frac{(p-q)(t_{i+1} - t^*)(t^* - t_i)}{t_{i+1} - t_i} \right| \leq |p-q| |t_{i+1} - t_i| = \frac{|p-q|}{m}.$$

Recall $t_i = \frac{i}{m}$ for all $i \in \{1, \dots, m\}$ and this upper bound tends to 0 as $m \rightarrow \infty$. \square

5.5 Proof of Lemma 5

Proof. Order the set \mathcal{T} as $\mathcal{T} = \{x_1, x_2, \dots, x_k\}$, and $x_i \leq x_{i+1}$ for all $1 \leq i \leq k-1$. Note $k \leq m+n$. Then on any $[x_i, x_{i+1}]$, f_1 and f_2 both are linear functions. Thus the function $f_1(x) - f_2(x)$ is also a linear function on $[x_i, x_{i+1}]$. Further we can verify that the function $|f_1(x) - f_2(x)|$ is convex on the compact and convex set $[x_i, x_{i+1}]$. Thus its maximum is obtained at some extreme point of the set $[x_1, x_{i+1}]$, which are $\{x_i, x_{i+1}\}$. We have,

$$\sup_{x \in [x_i, x_{i+1}]} |f_1(x) - f_2(x)| = \max\{|f_1(x_i) - f_2(x_i)|, |f_1(x_{i+1}) - f_2(x_{i+1})|\}.$$

This also holds on $[a, x_1]$ and $[x_k, b]$. Now we break the interval $[a, b]$ as $[a, b] = [a, x_1] \cup [x_1, x_2] \cdots \cup [x_k, b]$. Thus

$$\begin{aligned} \sup_{x \in [a, b]} |f_1(x) - f_2(x)| &= \max\left\{ \sup_{t \in [a, x_1]} |f_1(x) - f_2(x)|, \sup_{t \in [x_1, x_2]} |f_1(x) - f_2(x)|, \dots, \sup_{t \in [x_k, b]} |f_1(x) - f_2(x)| \right\} \\ &= \max\{|f_1(a) - f_2(a)|, \max_{x \in \mathcal{T}} |f_1(x) - f_2(x)|, |f_1(b) - f_2(b)|\}. \end{aligned}$$

□

5.6 Proof of Lemma 6

Proof. Without loss of generality, let's assume $0 < \hat{t} < t^*$. We state some key observations. First because $h \in \mathcal{S}(\{\hat{t}\})$, so we have:

$$\min_{f \in \mathcal{S}(\{\hat{t}\})} \sup_{t \in [0, T]} |f(t) - \psi(t)| \leq \sup_{t \in [0, T]} |h(t) - \psi(t)|.$$

And the left hand side is by Lemma 5:

$$\begin{aligned} \min_{f \in \mathcal{S}(\{\hat{t}\})} \sup_{t \in [0, T]} |f(t) - \psi(t)| &= \min_{\alpha, \beta_L, \beta_R, \beta_L \neq \beta_R} \sup_{t \in [0, T]} |\alpha + \beta_L(t - \hat{t}) + (\beta_R - \beta_L)(t - \hat{t})I_{\{t > \hat{t}\}} - \Delta(t - t^*)I_{\{t > t^*\}}| \\ &= \min_{\alpha, \beta_L, \beta_R, \beta_L \neq \beta_R} \max\{|\alpha|, |\alpha - \beta_L \hat{t}|, |\alpha + \beta_R(t^* - \hat{t})|, |\alpha + \beta_R(T - \hat{t}) - \Delta(T - t^*)|\}. \end{aligned}$$

By checking the KKT conditions (see 5.7), we obtain the minimum as $\frac{T-t^*}{2(T-\hat{t})}|\hat{t} - t^*|\Delta$. Thus we obtain that:

$$\frac{T-t^*}{2(T-\hat{t})}|\hat{t} - t^*|\Delta \leq \sup_{t \in [0, T]} |h(t) - \psi(t)|.$$

To bound the right hand side, we introduce $\psi^T(t)$ as the translation of $\psi(t)$ such that the changepoint is at the sampled time t_{k^*} that is closest to t^* , the changepoint of the true $\psi(t)$. That is:

$$\psi^T(t) = \Delta(t - t_{k^*})I_{\{t > t_{k^*}\}}.$$

Note $\psi^T(t) \in \mathcal{S}(\mathcal{T})$ and recall $\max_{t \in \mathcal{T}} |h - \hat{\psi}(t)| = \min_{f \in \mathcal{S}(\mathcal{T})} \max_{t \in \mathcal{T}} |f - \hat{\psi}(t)|$. Thus we have:

$$\max_{t \in \mathcal{T}} |h(t) - \hat{\psi}(t)| \leq \max_{t \in \mathcal{T}} |\psi^T(t) - \hat{\psi}(t)|.$$

We also have $\sup_{t \in [0, T]} |\psi^T(t) - \psi(t)| = \Delta|t^* - t_{k^*}| \leq \Delta\rho$.

Because $h(t) - \hat{\psi}(t)$ and $\psi^T(t) - \hat{\psi}(t)$ are both continuous piecewise linear functions with changepoints in \mathcal{T} , by Lemma 5 we have:

$$\max_{t \in \mathcal{T}} |h(t) - \hat{\psi}(t)| = \sup_{t \in [0, T]} |h(t) - \tilde{\psi}(t)|, \quad \max_{t \in \mathcal{T}} |\psi^T(t) - \hat{\psi}(t)| = \sup_{t \in [0, T]} |\psi^T(t) - \tilde{\psi}(t)|.$$

Thus

$$\sup_{t \in [0, T]} |h(t) - \tilde{\psi}(t)| \leq \sup_{t \in [0, T]} |\psi^T(t) - \tilde{\psi}(t)|. \quad (10)$$

Finally we have:

$$\begin{aligned} \frac{T - t^*}{2(T - \hat{t})} |\hat{t} - t^*| \Delta &\leq \sup_{t \in [0, T]} |h(t) - \psi(t)| \\ &\leq \sup_{t \in [0, T]} |h(t) - \tilde{\psi}(t)| + \sup_{t \in [0, T]} |\tilde{\psi}(t) - \psi(t)| \\ &\leq \sup_{t \in [0, T]} |\psi^T(t) - \tilde{\psi}(t)| + \sup_{t \in [0, T]} |\tilde{\psi}(t) - \psi(t)| \\ &\leq \sup_{t \in [0, T]} |\psi^T(t) - \psi(t)| + 2 \sup_{t \in [0, T]} |\tilde{\psi}(t) - \psi(t)| \\ &\leq \Delta \rho + 2 \sup_{t \in [0, T]} |\tilde{\psi}(t) - \psi(t)|. \end{aligned}$$

Dividing both sides with $\frac{T - t^*}{2(T - \hat{t})} \Delta$, then combine with $\frac{T - \hat{t}}{T - t^*} \leq \frac{T}{\min\{t^*, T - t^*\}}$, we get

$$|\hat{t} - t^*| \leq \left(\frac{4 \sup_{t \in [0, T]} |\tilde{\psi}(t) - \psi(t)|}{\Delta} + 2\rho \right) \frac{T}{\min\{T - t^*, t^*\}}.$$

Then for any given $\{\hat{\psi}(t_i) | 1 \leq i \leq m\}$ we can also use $\{-\hat{\psi}(t_i) | 1 \leq i \leq m\}$ for \hat{t} and it is the same as using $\{\hat{\psi}(t_i) | 1 \leq i \leq m\}$, thus we get

$$|\hat{t} - t^*| \leq \left(\frac{4 \sup_{t \in [0, T]} |-\tilde{\psi}(t) - \psi(t)|}{\Delta} + 2\rho \right) \frac{T}{\min\{T - t^*, t^*\}}.$$

Combining the above two results together we get

$$|\hat{t} - t^*| \leq \left(\frac{4 \min_{w \in \{\pm 1\}} \sup_{t \in [0, T]} |w\tilde{\psi}(t) - \psi(t)|}{\Delta} + 2\rho \right) \frac{T}{\min\{T - t^*, t^*\}}.$$

□

5.7 Verification of KKT condition

First we recall that KKT conditions are used in the study of constrained optimization problems. The minimizer of the constrained optimization problem must satisfy the KKT conditions, as the theorem stated below:

Theorem 10 (Necessary conditions for the minimizer). *Consider the constrained optimization problem:*

$$\begin{aligned} &\min f(\mathbf{x}) \\ &\text{subject to } g_1(\mathbf{x}) \leq 0 \\ &\quad \dots \\ &\quad g_k(\mathbf{x}) \leq 0 \end{aligned}$$

Suppose the minimizer of this problem is \mathbf{x}^* . If $g_{i_1}(\mathbf{x}^*) = g_{i_2}(\mathbf{x}^*) = \dots = g_{i_j}(\mathbf{x}^*) = 0$ (these are called active constraints), and $g_l(\mathbf{x}^*) < 0$ for $l \notin \{i_1, \dots, i_j\}$, then if the gradients of the active constraints evaluated at \mathbf{x}^* are linear independent, there exist $\lambda_1, \dots, \lambda_j \geq 0$ such that:

$$-\nabla f(\mathbf{x}^*) = \sum_{s=1}^j \lambda_s \nabla g_{i_s}(\mathbf{x}^*). \quad (11)$$

Our optimization problem is:

$$\min_{\alpha, \beta_L, \beta_R, \hat{t}} \max\{|\alpha|, |\alpha - \beta_L \hat{t}|, |\alpha + \beta_R(t^* - \hat{t})|, |\alpha + \beta_R(T - \hat{t}) - \Delta(T - t^*)|\}.$$

This is equivalent to:

$$\begin{aligned} \min f(z, \alpha, \beta_L, \beta_R) &= z; \\ \text{subject to } g_1 &= \alpha - z \leq 0, \\ g_2 &= -\alpha - z \leq 0, \\ g_3 &= \alpha - \beta_L \hat{t} - z \leq 0, \\ g_4 &= -\alpha + \beta_L \hat{t} - z \leq 0, \\ g_5 &= -\alpha - \beta_R(t^* - \hat{t}) - z \leq 0, \\ g_6 &= \alpha + \beta_R(t^* - \hat{t}) - z \leq 0, \\ g_7 &= -\alpha - \beta_R(T - \hat{t}) + \Delta(T - t^*) - z \leq 0, \\ g_8 &= \alpha + \beta_R(T - \hat{t}) - \Delta(T - t^*) - z \leq 0. \end{aligned}$$

We recall $\Delta > 0, 0 < \hat{t} < t^* < T$. Then

$$\nabla f(z, \alpha, \beta_L, \beta_R) = (1, 0, 0, 0)^\top.$$

Because $\nabla f(z, \alpha, \beta_L, \beta_R)$ is never 0, thus the minimizer \mathbf{x}^* must be on the boundary of the feasible set, that is, at least one of the constraints is active. In other words at least one of $g_i(\mathbf{x}^*) = 0$. In the following analysis, we will enumerate all possible sets of active constraints and find the only feasible ones, which yields the minimizer.

For demonstration we form a matrix ∇ with its i th column to be $\nabla g_i(z, \alpha, \beta_L, \beta_R)$:

$$\nabla = \begin{bmatrix} -1 & -1 & -1 & -1 & -1 & -1 & -1 & -1 \\ -1 & 1 & -1 & 1 & -1 & 1 & -1 & 1 \\ 0 & 0 & \hat{t} & -\hat{t} & 0 & 0 & 0 & 0 \\ 0 & 0 & 0 & 0 & -(t^* - \hat{t}) & t^* - \hat{t} & -(T - \hat{t}) & T - \hat{t} \end{bmatrix}.$$

Also if only one of the constraints are active at the minimizer, then by KKT conditions 10, there exists a $\lambda \geq 0$ such that:

$$\lambda \nabla g_i = (-1, 0, 0, 0)^\top.$$

This equation has no solution for any $i \in \{1, 2, \dots, 8\}$. Thus at least two of constraints are active at the minimizer. Also we note if any one of the four pairs of $(g_1, g_2), (g_3, g_4), (g_5, g_6), (g_7, g_8)$ are active, then $z = 0$, then $\Delta = 0$, which violates our assumption. Thus any pair of constraints mentioned above can only have one of them active.

Also note for g_3 and g_4 , because $\hat{t} > 0$ and only g_3 and g_4 has the third entry to be non-zero, so to satisfy the equation 11, the coefficients before ∇g_3 and ∇g_4 have to be equal. Since at most one of these coefficients is nonzero, they must both be 0.

Now we consider if the active constraints are among g_5, g_6, g_7, g_8 . Suppose the only constraints that are active are (g_5, g_7) (possibly g_3 or g_4 is also active but we have shown the corresponding coefficient is 0 so it won't influence the equation 11), then the equation 11 has no solution. Similarly we can show (g_6, g_8) can't be the only active constraints. Note that these arguments still go through if one of g_1, g_2 is active. Then for (g_5, g_8) to satisfy the equation 11, we find $T = t^*$ which again violates our assumption, and similarly for (g_6, g_7) . The above analysis shows that one of g_1 and g_2 has to be active, that is $z = \alpha$ or $z = -\alpha$.

Now consider (g_2, g_5, g_8) are all active, then we have:

$$z = -\alpha = -\alpha - \beta_R(t^* - \hat{t}) = \alpha + \beta_R(T - \hat{t}) - \Delta(T - t^*)$$

Thus $\beta_R = 0$ and $z = \frac{\Delta(t^*-T)}{2} < 0$, this is infeasible.
And for (g_1, g_5, g_8) we have:

$$z = \alpha = -\alpha - \beta_R(t^* - \hat{t}) = \alpha + \beta_R(T - \hat{t}) - \Delta(T - t^*)$$

Thus $\alpha = -\frac{\Delta(t^*-\hat{t})(T-t^*)}{2(T-\hat{t})}$, $z = -\frac{\Delta(t^*-\hat{t})(T-t^*)}{2(T-\hat{t})} < 0$, which is infeasible.

For (g_1, g_6, g_7) , by solving the active constraints similarly we have $z = \alpha = \frac{\Delta(T-t^*)}{2}$, this is feasible. Then we check the KKT condition 11:

$$\begin{cases} \lambda_1 + \lambda_6 + \lambda_7 = 1 \\ \lambda_1 + \lambda_6 - \lambda_7 = 0 \\ (t^* - \hat{t}) \lambda_6 - (T - \hat{t}) \lambda_7 = 0 \end{cases}$$

Solving it we note $\lambda_1 = \frac{1}{2} \left(1 - \frac{T-\hat{t}}{t^*-\hat{t}}\right) < 0$. Thus this violates the KKT conditions.

For (g_2, g_6, g_7) we have:

$$z = -\alpha = \alpha + \beta_R(t^* - \hat{t}) = -\alpha - \beta_R(T - \hat{t}) + \Delta(T - t^*)$$

Thus $\alpha = -\frac{\Delta(t^*-\hat{t})(T-t^*)}{2(T-\hat{t})}$, $z = \frac{\Delta(t^*-\hat{t})(T-t^*)}{2(T-\hat{t})}$. Then we check the KKT condition by solving the equations:

$$\begin{cases} \lambda_2 + \lambda_6 + \lambda_7 = 1 \\ -\lambda_2 + \lambda_6 - \lambda_7 = 0 \\ (t^* - \hat{t}) \lambda_6 - (T - \hat{t}) \lambda_7 = 0 \end{cases}$$

Thus we have solutions:

$$\begin{cases} \lambda_2 = \frac{1}{2} \left(1 - \frac{t^*-\hat{t}}{T-\hat{t}}\right) > 0 \\ \lambda_6 = \frac{1}{2} > 0 \\ \lambda_7 = \frac{t^*-\hat{t}}{2(T-\hat{t})} > 0 \end{cases}$$

This satisfies the KKT condition, and the corresponding gradients are linear independent:

$$\begin{bmatrix} -1 & -1 & -1 \\ 1 & 1 & -1 \\ 0 & 0 & 0 \\ 0 & t^* - \hat{t} & -(T - \hat{t}) \end{bmatrix}$$

Because these active constraints at the minimizer are the only set that satisfies the KKT conditions (with the possible addition of g_3 or g_4), and these active constraints yield that $z = \frac{\Delta(t^*-\hat{t})(T-t^*)}{2(T-\hat{t})}$. We conclude the minimum value of this optimization problem is $\frac{\Delta(t^*-\hat{t})(T-t^*)}{2(T-\hat{t})}$.

5.8 Proof of Theorem 5

First we state a useful lemma.

Lemma 7. *Assume that $\psi(t)$ is an α -Hölder continuous with constant L function on $t \in [0, T]$. Let the sampled times $\{t_1, t_2, \dots, t_m\} \subset [0, T]$ be given and without loss of generality we assume $t_1 = 0$ and $t_m = T$. Denote*

$$\max_{1 \leq i < m} |t_i - t_{i+1}|^\alpha = \rho.$$

If $\tilde{\psi}(t)$ is the piecewise linear interpolation between the points $\{(t_i, \psi(t_i)), 1 \leq i \leq m\}$, then

$$\sup_{t \in [0, T]} |\tilde{\psi}(t) - \psi(t)| \leq \rho L.$$

Proof. For $t \in [0, T]$ and $t \neq t_k$ for $1 \leq k \leq m$, because we assume $t_1 = 0$ and $t_m = T$, we can always find t_i and t_{i+1} where $1 \leq i < m$ such that $t \in (t_i, t_{i+1})$. Then there exist a $0 < \lambda < 1$ such that $t = \lambda t_i + (1 - \lambda)t_{i+1}$. Since $\tilde{\psi}(t)$ is the piecewise linear interpolation between the points $\{(t_i, \psi(t_i)), 1 \leq i \leq m\}$, it follows that

$$\tilde{\psi}(t) = \lambda \psi(t_i) + (1 - \lambda) \psi(t_{i+1}).$$

We thus have

$$\begin{aligned} |\tilde{\psi}(t) - \psi(t)| &= |\lambda(\psi(t_i) - \psi(t)) + (1 - \lambda)(\psi(t_{i+1}) - \psi(t))| \\ &\leq \lambda L |t - t_i|^\alpha + (1 - \lambda)L |t_{i+1} - t|^\alpha \\ &\leq (\lambda L + (1 - \lambda)L) |t_{i+1} - t_i|^\alpha \\ &= L |t_i - t_{i+1}|^\alpha. \end{aligned}$$

Thus

$$\sup_{0 \leq t \leq T} |\tilde{\psi}(t) - \psi(t)| \leq L \max_{1 \leq i < m} |t_i - t_{i+1}|^\alpha = \rho L.$$

□

Now we are ready to prove Theorem 5. We know there exists a $w_m \in \{\pm 1\}$ such that

$$\begin{aligned} \sup_{t \in [0, T]} |\tilde{\psi}(t) - w_m \psi(t)| &\leq \sup_{t \in [0, T]} |\tilde{\psi}(t) - w_m \tilde{\psi}(t)| + \sup_{t \in [0, T]} |w_m \tilde{\psi}(t) - w_m \psi(t)|, \\ &\leq \max_{1 \leq i \leq m} |\hat{\psi}(t_i) - w_m \psi(t_i)| + \rho L, \quad (\text{by Lemma 7 and Lemma 5}) \\ &\leq C \frac{m \log(n)}{\sqrt{n} \lambda_1(-\frac{1}{2} P \mathcal{D}^{(2)} P)} + \rho L, \quad (\text{by Theorem 4}) \end{aligned}$$

so the result follows.

5.9 Proof of Theorem 6

Proof. $\psi(t) = \Delta(t - t^*) I_{\{t > t^*\}}$ for $t \in [0, T]$, thus $\psi(t)$ is Lipschitz continuous with constant Δ . Also note for any $w_m \in \{\pm 1\}$, $\min_{w \in \{\pm 1\}} \sup_{t \in [0, T]} |\tilde{\psi}(t) - w \psi(t)| \leq \sup_{t \in [0, T]} |\tilde{\psi}(t) - w_m \psi(t)|$. Thus combining Theorem 5 and Lemma 6 gives the result.

We show that $\lambda_1(-\frac{1}{2} P \mathcal{D}^{(2)} P) = (\sum_{i=1}^m \psi_{centered}^2(t_i))$, where $\mathcal{D}^{(2)}$ is entrywise square of the distance matrix of the mirror $\psi(t) = \Delta(t - t^*) I_{\{t > t^*\}}$, $t \in [0, T]$. Denote

$$\Psi_m = (\psi_{centered}(t_1), \psi_{centered}(t_2), \dots, \psi_{centered}(t_m))$$

as the $m \times 1$ vector, where $\psi_{centered}(t)$ satisfies that $\sum_0^T \psi_{centered}(t) dt = 0$. Additionally, in our case: $\psi_{centered}(t) = \Delta(t - t^*) I_{\{t > t^*\}} + \Delta(t^* - \frac{T^2 - (t^*)^2}{2T})$. Thus

$$-\frac{1}{2} P \mathcal{D}^{(2)} P = \Psi_m \Psi_m^\top.$$

So $\lambda_1(-\frac{1}{2} P \mathcal{D}^{(2)} P) = \lambda_1(\Psi_m \Psi_m^\top) = \Psi_m^\top \Psi_m = \sum_{i=1}^m \psi_{centered}^2(t_i)$. □

5.10 Proof of Corollary 1

Proof. In this case $\rho = \frac{T}{m-1}$. First we center the $\psi(t)$ then

$$\begin{aligned} \frac{1}{m} \sum_{i=1}^m \psi_{centered}^2(t_i) &= \frac{m-1}{mT} \sum_{i=2}^m \frac{T}{m-1} \psi_{centered}^2\left(\frac{(i-1)T}{m-1}\right) \\ &\rightarrow \frac{1}{T} \int_0^T \psi_{centered}^2(t) dt \\ &= \Delta^2 \left(1 - \frac{t^*}{T}\right)^3 \frac{(3t^* + T)T}{12}. \end{aligned}$$

plug this back in we get the result. \square

5.11 Proof of Theorem 7

Proof.

$$\sup_{t \in [0, T]} |\tilde{\psi}_1^{(m)}(t) - w'_m \psi_0(t)| \leq \sup_{t \in [0, T]} |\tilde{\psi}_1^{(m)}(t) - w_m \tilde{\psi}_1^{(m)}(t)| + \sup_{t \in [0, T]} |w_m \tilde{\psi}_1^{(m)}(t) - w'_m \psi_0(t)|.$$

We need two different $w_m \in \{\pm 1\}$ and $w'_m \in \{\pm 1\}$ here to account for the nonidentifiability between $\hat{\psi}_1^{(m)}$ and $\psi_1^{(m)}$ and the nonidentifiability between $\psi_1^{(m)}$ and ψ_0 . To bound the first term we apply Lemma 5,

$$\sup_{t \in [0, T]} |\tilde{\psi}_1^{(m)}(t) - w_m \tilde{\psi}_1^{(m)}(t)| \leq \max_{1 \leq i \leq m} |\hat{\psi}_1^{(m)}(t_i) - w_m \psi_1^{(m)}(t_i)|,$$

and from Theorem 4, we know there exists a $w_m \in \{\pm 1\}$ and a constant C such that with high probability:

$$\max_{1 \leq i \leq m} |\hat{\psi}_1^{(m)}(t_i) - w_m \psi_1^{(m)}(t_i)| \leq C \left(\frac{m \log(n)}{\sqrt{n} \lambda_1 \left(-\frac{1}{2} PD^{(2)} P\right)} + \frac{\sqrt{\sum_{i=2}^m \lambda_i^2 \left(-\frac{1}{2} PD^{(2)} P\right)}}{\lambda_1 \left(-\frac{1}{2} PD^{(2)} P\right)} \right).$$

\square

5.12 Beyond the first dimension

The consistency results discussed previously hinge on the assumption for the mirror of asymptotic piecewise linearity in the first dimension, with the influences in all other dimensions diminishing. However, as observed in Fig 3, the changepoints are preserved in the deeper dimensions. To see this more precisely, let's revisit the distance matrix for Model 3. Recall in Lemma 2,

$$\left(\mathcal{D}_{\varphi_m}^{(2)}\right)_{i,j} = \begin{cases} \frac{p^2}{m^2} (i-j)^2 + \frac{p-p^2}{m^2} |i-j| & i, j < t_m^* \\ \left(\frac{p}{m} (t_m^* - i) + \frac{q}{m} (j - t_m^*)\right)^2 + \frac{p-p^2}{m^2} (t_m^* - i) + \frac{q-q^2}{m^2} (j - t_m^*) & i < t_m^* < j \\ \frac{q^2}{m^2} (j-i)^2 + \frac{q-q^2}{m^2} |i-j| & t_m^* < i, j \end{cases}.$$

To study the mirror of Model 3, we perform CMDS on this distance matrix, which amounts to taking an eigendecomposition of $-\frac{1}{2} P \mathcal{D}_{\varphi_m}^{(2)} P$. When m is large, this eigendecomposition can be approximated through the kernel method of Diaconis et al. [2008], in which we consider a kernel function $\kappa^m(x, y)$ that provides a continuous-time analogue of the discrete distance matrix, and a double-centering operator that approximates the discrete centering with an integral.

To that end we define a corresponding kernel function $\kappa^m(x, y) : [0, 1]^2 \rightarrow \mathbb{R}$:

$$\kappa^m(x, y) = \begin{cases} p^2(x-y)^2 + \frac{p-p^2}{m}|x-y| & x, y < t^* \\ (t^* - x)^2 p^2 + \frac{p-p^2}{m}(t^* - x) + (y - t^*)^2 q^2 + \frac{q-q^2}{m}(y - t^*) + 2pq(y - t^*)(t^* - x) & x < t^* < y \\ (t^* - y)^2 p^2 + \frac{p-p^2}{m}(t^* - y) + (x - t^*)^2 q^2 + \frac{q-q^2}{m}(x - t^*) + 2pq(x - t^*)(t^* - y) & y < t^* < x \\ q^2(x-y)^2 + \frac{q-q^2}{m}|x-y| & t^* < x, y \quad \text{where } t^* = \frac{t_m^*}{m}, \end{cases}$$

and a double-centering operator \mathcal{DC} :

$$\mathcal{DC}[\kappa(x, y)] := \kappa(x, y) - \int_0^1 \kappa(x, y) dx - \int_0^1 \kappa(x, y) dy + \int_0^1 \int_0^1 \kappa(x, y) dx dy.$$

Then the continuous time-time analogue of $PD_{\varphi_m}^{(2)}P$ is $\mathcal{DC}[\kappa^m(x, y)] =$

$$\left\{ \begin{array}{l} p^2 \left((2t_m^* - t_m^{*2})(x+y) - 2xy \right) + \frac{p-p^2}{m} (|x-y| - x^2 - y^2 + x+y) + pq(1 - t_m^{*2})(x+y) + c_1, \\ \hspace{25em} x, y < t_m^*; \\ -p^2 t_m^{*2} x - \frac{p-p^2}{m} x^2 + q^2 (t_m^* - 1)^2 y + \frac{q-q^2}{m} (2y - y^2) \\ \quad + pq \left(-2xy + (2t_m^* - t_m^{*2})y + (-t_m^{*2} + 2t_m^* + 1)x \right) + c_2, \quad x < t_m^* < y; \\ -p^2 t_m^{*2} y - \frac{p-p^2}{m} y^2 + q^2 (t_m^* - 1)^2 x + \frac{q-q^2}{m} (2x - x^2) \\ \quad + pq \left(-2xy + (2t_m^* - t_m^{*2})x + (-t_m^{*2} + 2t_m^* + 1)y \right) + c_2, \quad y < t_m^* < x; \\ q^2 \left((2t_m^* - t_m^{*2})(x+y) - 2xy \right) + \frac{q-q^2}{m} (|x-y| - x^2 - y^2 + x+y) + pq(1 - t_m^{*2})(x+y) + c_3, \\ \hspace{25em} x, y > t_m^*; \end{array} \right. \quad (12)$$

where c_1, c_2, c_3 are constants.

Observe that each of these kernels induces an associated integral operator $I_\kappa : L^2([0, 1]) \rightarrow L^2([0, 1])$ defined by

$$I_\kappa[f](x) = \int_0^1 \kappa(x, y) f(y) dy.$$

The κ_c^m kernel defined as $\kappa_c^m(x, y) := -\frac{1}{2}\mathcal{DC}[\kappa^m(x, y)]$ can approximate our doubly-centered matrix, as follows.

Lemma 8. *With κ_c^m defined as $\kappa_c^m(x, y) := -\frac{1}{2}\mathcal{DC}[\kappa^m(x, y)]$, define a matrix S with its i, j entry as:*

$$S_{i,j} := \kappa_c^m \left(\frac{i}{m}, \frac{j}{m} \right).$$

Then for large m we have

$$\max_{1 \leq i \leq m, 1 \leq j \leq m} \left| S_{i,j} - \left(-\frac{1}{2} PD_{\varphi_m}^{(2)} P \right)_{i,j} \right| \sim \Theta \left(\frac{1}{m} \right).$$

For an integral operator I_κ , its eigenvalues λ and eigenfunctions $f \in L^2([0, 1])$ satisfy that:

$$I_\kappa[f](x) = \lambda f(x) \quad \text{for all } x \in [0, 1].$$

In the following theorem we show an explicit form for the eigenfunction of the integral operator $I_{\kappa_c^m}$, which can be considered as an approximate of the eigenvectors of our doubly-centered matrix.

Theorem 11. *For the kernel function $\kappa_c^m(x, y) = -\frac{1}{2}\mathcal{DC}[\kappa^m(x, y)]$ where $\mathcal{DC}[\kappa^m(x, y)]$ is defined in Equation 12, any eigenfunction of its corresponding integral operator $I_{\kappa_c^m}$ must take the following form:*

$$k(x) = \begin{cases} A_{\text{pre}} \cos\left(\sqrt{\frac{p(1-p)}{m\lambda}}x\right) + B_{\text{pre}} \sin\left(\sqrt{\frac{p(1-p)}{m\lambda}}x\right) & \text{for } x \leq t^* \\ A_{\text{post}} \cos\left(\sqrt{\frac{q(1-q)}{m\lambda}}x\right) + B_{\text{post}} \sin\left(\sqrt{\frac{q(1-q)}{m\lambda}}x\right) & \text{for } x > t^*, \end{cases}$$

where λ , A_{pre} , B_{pre} and A_{post} , B_{post} are real numbers and satisfy $\int_0^1 k(t)dt = 0$, $\int_0^1 k^2(t)dt = 1$. Thus, the approximated mirror for Model 3 will be $k(x)$ scaled by the square root of the eigenvalues.

Determining λ , A_{pre} , B_{pre} and A_{post} , B_{post} requires solution of an especially complicated equation, but an explicit solution is unnecessary. Rather, the key is that Theorem 11 demonstrates that there is a change in frequency at t^* in all eigenfunctions, making the estimated eigenvectors in all dimensions a useful object of study for changepoint localization.

As shown in Figure 4, in the first dimension of the estimated mirror, we observe the approximate linearity property with a slope change at t^* . The second and third dimensions also exhibit a change in behavior at t^* , where the frequency of the cosine and sine curves changes abruptly at this point. This means that even if the dimension of the estimated mirror is chosen to be too large, the corresponding eigenfunctions continue to add to the evidence for a changepoint at t^* but with bigger variance. We will further illustrate this bias-variance trade off phenomenon in the following numerical experiments section.

5.13 Proof of Lemma 8

Proof. Consider the function $\kappa^m(x, y)$ as defined in Section 5.12. Note this function is bounded on $[0, 1] \times [0, 1]$. Putting $x_i = i/m$, we observe

$$\kappa^m(x_i, x_j) = (\mathcal{D}_{\varphi_m}^{(2)})_{i,j}.$$

Also recall $P = I - \frac{J}{m}$ and J is an all ones matrix thus $P\mathcal{D}_{\varphi_m}^{(2)}P = \mathcal{D}_{\varphi_m}^{(2)} - \frac{1}{m}J\mathcal{D}_{\varphi_m}^{(2)} - \frac{1}{m}\mathcal{D}_{\varphi_m}^{(2)}J + \frac{1}{m^2}J\mathcal{D}_{\varphi_m}^{(2)}J$. We quote the well-known error bound for right hand rule here:

Lemma 9 (Right hand rule error bound for numerical integration). *Suppose that $f(x)$ is differentiable on $[a, b]$ and $|f'(x)| \leq K_1$, then*

$$\int_a^b f(x)dx = \sum_{i=1}^m \frac{b-a}{m} f\left(\frac{i}{m}\right) + E_R \quad \text{where} \quad |E_R| \leq \frac{K_1(b-a)^2}{2m} \quad K_1 = \max_{x \in [a,b]} |f'(x)|.$$

We find

$$\left(\frac{1}{m}J\mathcal{D}_{\varphi}^{(2)}\right)_{i,j} = \sum_{t=1}^m \frac{1}{m} (\mathcal{D}_{\varphi}^{(2)})_{t,j} = \sum_{t=1}^m \frac{1}{m} \kappa^m\left(\frac{t}{m}, x_j\right),$$

and

$$\begin{aligned} \sum_{t=1}^m \frac{1}{m} \kappa^m\left(\frac{t}{m}, x_j\right) &= \sum_{t=1}^{t_m^*} \frac{1}{m} \kappa^m\left(\frac{t}{m}, x_j\right) + \sum_{t=t_m^*+1}^m \frac{1}{m} \kappa^m\left(\frac{t}{m}, x_j\right) \\ &= \int_0^{t^*} \kappa^m(x, x_j)dx + R_{x_j}^{(1)} + \int_{t^*}^1 \kappa^m(x, x_j)dx + R'_{x_j}. \end{aligned}$$

Note here we apply the right hand rule error bound because $\kappa^m(x, y)$ is differentiable with respect to x on $[0, t^*]$ for any fixed $y \in [0, 1]$ and differentiable with respect to x on $[t^*, 1]$ for any fixed $y \in [0, 1]$. Further we have $\frac{d\kappa^m(x, y)}{dx}$ on $x \in [0, t^*]$ is bounded for any $y \in [0, 1]$ and same for $\frac{d\kappa^m(x, y)}{dx}$ on $x \in [t^*, 1]$. Thus by the Lemma we know

$$R_{x_j}^{(1)} \leq \frac{\max_{x \in [0, t^*]} \left| \frac{d\kappa^m(x, y)}{dx} \right|}{2m} \leq \frac{\max_{y \in [0, 1]} \max_{x \in [0, t^*]} \left| \frac{d\kappa^m(x, y)}{dx} \right|}{2m} \leq \frac{C}{m} \quad \text{for } \forall x_j \in [0, 1].$$

And the same holds for R'_{x_j} . Thus we gain an uniform upper bound for the right hand error:

$$\forall x_j \in [0, 1] \quad \sum_{t=1}^m \frac{1}{m} \kappa \left(\frac{t}{m}, x_j \right) = \int_0^1 \kappa(x, x_j) dx + R^{(1)} \quad \text{where } |R^{(1)}| \sim O \left(\frac{1}{m} \right).$$

For

$$\left(\frac{1}{m} \mathcal{D}_{\varphi}^{(2)} J \right)_{i,j} = \sum_{t=1}^m \frac{1}{m} \left(\mathcal{D}_{\varphi}^{(2)} \right)_{i,t} = \sum_{t=1}^m \frac{1}{m} \kappa \left(x_i, \frac{t}{m} \right),$$

since $\kappa^m(x, y)$ is symmetric we have the same thing holds:

$$\forall x_i \in [0, 1] \quad \sum_{t=1}^m \frac{1}{m} \kappa^m \left(x_i, \frac{t}{m} \right) = \int_0^1 \kappa^m(x_i, x) dx + R^{(2)} \quad \text{where } |R^{(2)}| \sim O \left(\frac{1}{m} \right)$$

Now for

$$\left(\frac{1}{m^2} J \mathcal{D}_{\varphi_m}^{(2)} J \right)_{i,j} = \sum_{t'=1}^m \sum_{t=1}^m \frac{1}{m^2} \left(\mathcal{D}_{\varphi_m}^{(2)} \right)_{t',t} = \sum_{t'=1}^m \sum_{t=1}^m \frac{1}{m^2} \kappa \left(\frac{t'}{m}, \frac{t}{m} \right),$$

we find

$$\begin{aligned} \sum_{t'=1}^m \sum_{t=1}^m \frac{1}{m^2} \kappa^m \left(\frac{t'}{m}, \frac{t}{m} \right) &= \sum_{t'=1}^m \frac{1}{m} \left(\sum_{t=1}^m \frac{1}{m} \kappa^m \left(x_{t'}, \frac{t}{m} \right) \right), \\ &= \sum_{t'=1}^m \frac{1}{m} \left(\int_0^1 \kappa(x_{t'}, y) dy + R^{(2)} \right), \\ &= \sum_{t'=1}^m \frac{1}{m} \int_0^1 \kappa^m(x_{t'}, y) dy + \sum_{t'=1}^m \frac{1}{m} R^{(2)}, \\ &= \int_0^1 \int_0^1 \kappa(x, y) dx dy + R^{(3)} + R^{(2)}, \\ &\quad \text{where } R^{(3)} \leq \frac{\max_{x \in [0, 1]} \left| \frac{d \int_0^1 \kappa^m(x, y) dy}{dx} \right|}{2m} \sim O \left(\frac{1}{m} \right). \end{aligned}$$

Then for any $i, j \in \{1, 2, \dots, m\}$:

$$\begin{aligned} \left(-\frac{1}{2} P \mathcal{D}_{\varphi_m}^{(2)} P \right)_{i,j} &= -\frac{1}{2} \left(\mathcal{D}_{\varphi_m}^{(2)} - \frac{1}{m} J \mathcal{D}_{\varphi_m}^{(2)} - \frac{1}{m} \mathcal{D}_{\varphi_m}^{(2)} J + \frac{1}{m^2} J \mathcal{D}_{\varphi_m}^{(2)} J \right)_{i,j} \\ &= -\frac{1}{2} \left[\kappa^m(x_i, x_j) - \int_0^1 \kappa^m(x, x_j) dx - \int_0^1 \kappa^m(x_i, y) dy + \int_0^1 \int_0^1 \kappa^m(x, y) dx dy \right. \\ &\quad \left. - R^{(1)} - R^{(2)} + R^{(3)} + R^{(2)} \right]. \end{aligned}$$

Recall $\kappa_c^m(x_i, x_j) = \frac{1}{2} [\kappa(x_i, x_j) - \int_0^1 \kappa^m(x, x_j) dx - \int_0^1 \kappa(x_i, y) dy + \int_0^1 \int_0^1 \kappa(x, y) dx dy]$. Then we have:

$$\left| \left(-\frac{1}{2} P \mathcal{D}_{\varphi}^{(2)} P \right)_{i,j} - \kappa_c^m(x_i, x_j) \right| = \frac{1}{2} \left| -R^{(1)} - R^{(2)} + R^{(3)} + R^{(2)} \right| \sim O \left(\frac{1}{m} \right) \quad \forall x_i, x_j \in [0, 1].$$

This completes our proof. \square

5.14 Proof of Theorem 11

Proof. Consider a function $f(y) = g(y)$ for $y \leq t^*$, $f(y) = h(y)$ for $y > t^*$, where $g(t^*) = h(t^*)$. If f is an eigenvector of the integral operator induced by κ_c^m , then

$$\begin{aligned}
 & -\frac{1}{2} \int_0^1 \mathcal{DC}[\kappa^m(x, y)]f(y) \, dy = \lambda f(x), \text{ so} \\
 (x < t^*) : & \int_0^{t^*} \mathcal{DC}[\kappa^m(x, y)]g(y) \, dy + \int_{t^*}^1 \mathcal{DC}[\kappa^m(x, y)]h(y) \, dy = -2\lambda g(x) \\
 (x > t^*) : & \int_0^{t^*} \mathcal{DC}[\kappa^m(x, y)]g(y) \, dy + \int_{t^*}^1 \mathcal{DC}[\kappa^m(x, y)]h(y) \, dy = -2\lambda h(x).
 \end{aligned}$$

We consider taking the derivative with respect to x twice on both sides of these equations.

$$\begin{aligned}
 (x < t^*) : & \frac{\partial^2}{\partial x^2} \int_0^{t^*} \mathcal{DC}[\kappa^m(x, y)]g(y) \, dy \\
 & = \int_0^{t^*} \frac{p-p^2}{m}(-2)g(y) \, dy \\
 & + \frac{\partial^2}{\partial x^2} \int_0^x \frac{p-p^2}{m}(x-y)g(y) \, dy + \int_x^{t^*} \frac{p-p^2}{m}(y-x)g(y) \, dy \\
 & = \frac{p-p^2}{m}(-2)[G(t^*) - G(0)] \\
 & + \frac{\partial}{\partial x} \int_0^x \frac{p-p^2}{m}g(y) \, dy + \int_x^{t^*} \frac{p-p^2}{m}(-1)g(y) \, dy \\
 & = \frac{p-p^2}{m} [(-2)(G(t^*) - G(0)) + 2g(x)] \\
 (x < t^*) : & \frac{\partial^2}{\partial x^2} \int_{t^*}^1 \mathcal{DC}[\kappa^m(x, y)]h(y) \, dy \\
 & = \int_{t^*}^1 \frac{p-p^2}{m}(-2)h(y) \, dy \\
 & = \frac{p-p^2}{m}(-2)[H(1) - H(t^*)]
 \end{aligned}$$

We observe that $G(t^*) - G(0) + H(1) - H(t^*) = \int_0^{t^*} g(y) \, dy + \int_{t^*}^1 h(y) \, dy = \int_0^1 f(y) \, dy = 0$, so the first equation (for $x < t^*$) reads

$$\frac{2p(1-p)}{m}g(x) = -2\lambda g''(x).$$

For the second equation,

$$\begin{aligned}
(x > t^*) : & \frac{\partial^2}{\partial x^2} \int_0^{t^*} \mathcal{DC}[\kappa^m(x, y)]g(y) \, dy \\
& = \int_0^{t^*} \frac{q - q^2}{m} (-2)g(y) \, dy \\
& = \frac{q - q^2}{m} (-2)[G(t^*) - G(0)] \\
(x > t^*) : & \frac{\partial^2}{\partial x^2} \int_{t^*}^1 \mathcal{DC}[\kappa^m(x, y)]h(y) \, dy \\
& = \int_{t^*}^1 \frac{q - q^2}{m} (-2)h(y) \, dy \\
& + \frac{\partial^2}{\partial x^2} \int_{t^*}^x \frac{q - q^2}{m} (x - y)h(y) \, dy + \int_x^1 \frac{q - q^2}{m} (y - x)h(y) \, dy \\
& = \frac{q - q^2}{m} (-2)[H(1) - H(t^*)] \\
& + \frac{\partial}{\partial x} \int_{t^*}^x \frac{q - q^2}{m} h(y) \, dy + \int_x^1 \frac{q - q^2}{m} (-1)h(y) \, dy \\
& = \frac{q - q^2}{m} [(-2)(H(1) - H(t^*)) + 2h(x)]
\end{aligned}$$

Again applying the condition $\int_0^1 f(y) \, dy = 0$, the second equation (for $x > t^*$) reads

$$\frac{2q(1 - q)}{m} h(x) = -2\lambda h''(x).$$

The solutions to the differential equation for g must have the form e^{rx} where r is a root of the equation $r^2 + \frac{p(1-p)}{m\lambda} = 0$. In other words, $r = \pm i\sqrt{\frac{p(1-p)}{m\lambda}}$ (Assuming $\lambda > 0$). Arguing similarly for h , we see that the solutions must have the form:

$$\begin{aligned}
g(x) & = A_g \cos\left(\sqrt{\frac{p(1-p)}{m\lambda}}x\right) + B_g \sin\left(\sqrt{\frac{p(1-p)}{m\lambda}}x\right) \\
h(x) & = A_h \cos\left(\sqrt{\frac{q(1-q)}{m\lambda}}x\right) + B_h \sin\left(\sqrt{\frac{q(1-q)}{m\lambda}}x\right).
\end{aligned}$$

□